Development of Aptamer-Based Biolayer Interferometry Biosensors for the Detection of Cancer and Viral Biomarkers

Elnaz Yaghoobi

Thesis submitted to the University of Ottawa in partial fulfillment of the requirements for the Master's degree in chemistry

Department of Chemistry and Biomolecular Sciences

Faculty of Science

University of Ottawa

Abstract

This thesis used Biolayer Interferometry (BLI) and DNA aptamers to develop simple and reliable biosensors for detecting important biological targets, including proteins, cancer-derived exosomes, and viral-like particles (VLPs), ranked from simple to complex biomolecules. Aptamers are short single-stranded DNA molecules that can be considered as a bio recognition element that are able to specifically recognize proteins or particles, similar to antibodies but with better stability and easier preparation. This study sought to develop a rapid, sensitive, and label-free technology for quantitative detection by integrating aptamers with the BLI method, which enables real-time monitoring of molecular interactions without the need for labels. In the first project, an aptamer designed for the Ki-67 protein, a known marker of cell proliferation, was studied using a BLI platform. The results showed a strong and preferable specific interaction between the aptamer and Ki-67 protein, with a dissociation constant (K_D) of 10.9 ± 0.6 nM and a clear linear relationship across the working range of 50–400 nM. This confirmed that the BLI-based aptasensor can provide accurate and reproducible data for protein detection. The second project focused on the detection of cancer-derived exosomes from MDA-MB-231 cells using three known aptamers: CD63, MUC1, and 5TR1. Exosomes were isolated through a gold standard isolation method which is ultracentrifugation and characterized by Dynamic Light Scattering (DLS) and Transmission Electron Microscopy (TEM), which confirmed their typical size and structure. The binding tests showed that all three aptamers interacted strongly with exosomes, with K_D values in the picomolar range and good linearity in the calibration plots. These results demonstrated the high sensitivity and specificity of the aptamer-based BLI system for exosome analysis. In the third project, newly selected aptamers were tested for recognizing SARS-CoV-2 pseudoviruses (VLPs). Among them, the S1-SP10 aptamer showed the best performance with a K_D of 112 ± 5 nM and a limit of detection

(LOD) of 33 nM. The assay showed clear dose-dependent signals and high specificity compared to the scrambled control sequence, confirming that the aptamer could effectively bind the viral spike protein in its native form.

Overall, this research shows that BLI combined with aptamers is a powerful and flexible approach for studying molecular interactions and detecting disease-related biomarkers. The developed aptasensors worked well for different biological systems, proteins, exosomes, and viral particles, proving their potential for future use in medical diagnostics and real-sample testing.

Acknowledgments

First and foremost, I would like to thank myself for staying strong and determined throughout this challenging journey. Completing this work required patience, resilience, and countless hours of effort, and I am proud of how I kept moving forward even when the path was not easy.

My deepest gratitude goes to my husband, whose unwavering belief in me has been my greatest source of motivation. He has always seen my potential, encouraged me to pursue my goals, and stood beside me through every difficulty with love and understanding. His support has been my strength and comfort in times of doubt.

I would also like to express my heartfelt thanks to my parents. Even though they are far away, their love, prayers, and encouragement have been constant sources of hope and inspiration. Their belief in my dreams has given me the courage to follow them, no matter how far life has taken me from home.

Table of Contents

List of Figures

List of Tables

Chapter 1

Introduction

1.1 Aptamers

The term "*aptamer"* originates from the Latin word "*aptus"*, which means "to fit" a name that captures the highly selective binding behavior of these short nucleic acid sequences. The idea of using synthetic nucleic acids as molecular recognition elements emerged in the early 1990s, when Ellington and Szostak showed that laboratory-generated RNA strands could recognize and bind small dye molecules with high specificity. Building on this discovery, Tuerk and Gold soon introduced a selection approach based on iterative amplification and enrichment, later termed Systematic Evolution of Ligands by Exponential Enrichment (SELEX), which laid the groundwork for the systematic generation of aptamers[1, 2]. Aptamers are short single-stranded oligonucleotides typically made of DNA or RNA, capable of binding target molecules with a high level of affinity and specificity. Aptamers recognize their targets by folding into unique three-dimensional structures that physically and chemically match the target surface, allowing them to distinguish even very similar biomolecules through subtle differences in shape and charge. Therefore, the structural flexibility of aptamers facilitates tight and specific binding to target molecules. The high selectivity of aptamers contributes to improved analytical specificity by

limiting false-positive responses; however, this advantage is only fully realized when surface immobilization strategies are carefully designed to avoid steric constraints or partial masking of binding regions that may otherwise lead to false-negative signals[3]. Unlike biologically produced receptors, aptamers are generated through chemical synthesis, enabling precise sequence definition and high batch-to-batch reproducibility, thereby reducing variability associated with biological expression systems[4]. Their nucleic acid composition also imparts enhanced resistance to chemical and thermal stress, allowing aptamers to retain structural integrity and binding function under experimental conditions that can compromise antibody stability[5]. While aptamers are often proposed as alternatives to antibodies due to advantages such as lower production costs, straightforward chemical modification, and reversible thermal denaturation, their practical performance must still be validated for each target and application[6]. In comparison with protein-based receptors, aptamers generally display reduced susceptibility to irreversible denaturation and can be rationally engineered to control surface orientation and probe density, which is critical for achieving reproducible sensor performance. Notably, well-optimized aptamers can exhibit dissociation constants in the nanomolar to picomolar range, comparable to those of high-affinity monoclonal antibodies[7]. Collectively, these attributes support the suitability of aptamers for biosensing in complex biological matrices, where non-specific adsorption and surface biofouling frequently undermine analytical reliability[8, 9].

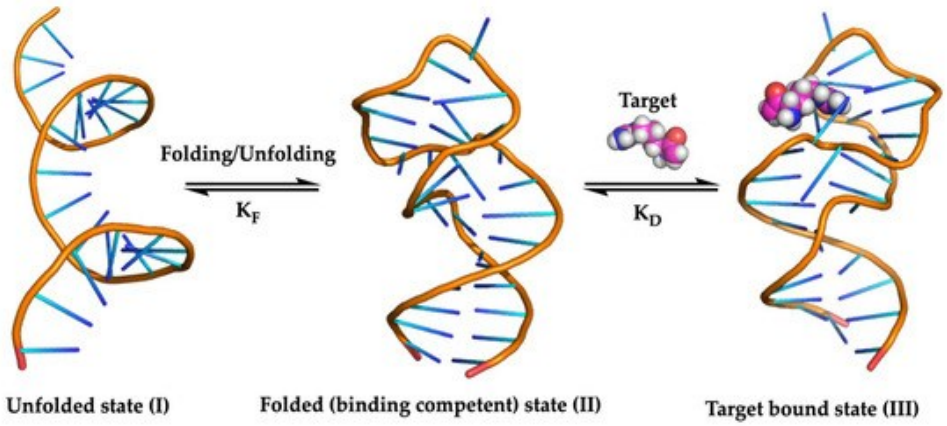

Figure 1. Visualization of the aptamer along with its target interaction region. Reprinted from J.P. Elskens et Al. Int. J. Mol. Sci. 2020, 21(12), 4522, under the Creative Commons (CC BY) license[10].

1.1.1 Systematic Evolution of Ligand Exponential Enrichment (SELEX)

Aptamers are selected from an *in vitro* procedure called Systematic Evolution of Ligands by EXponential enrichment (SELEX)[11]. The conventional SELEX process, summarized in (Figure 2), can be divided into three key steps. First, a library of randomized single-stranded nucleic acids is created. Next, this library is subjected to target binding, followed by the removal of non-binding strands and recovery of those that relate to the target. Finally, the collected sequences are amplified by PCR. Repeating these steps of binding, separation, and amplification (generally 5 to 15 cycles), results in aptamers with enhanced binding specificity and affinity [4, 12, 13].Several variations of the SELEX procedure have been developed for the refinement of aptamers.

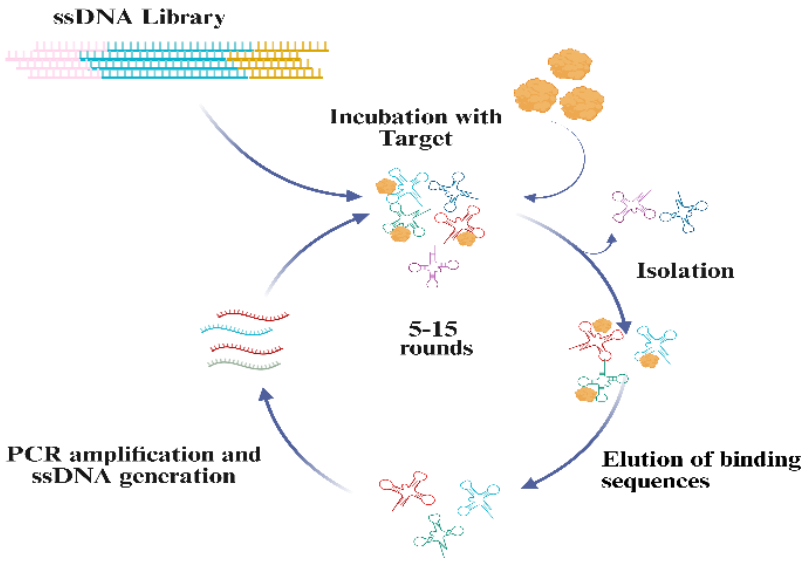

Figure 2.General workflow of SELEX. The process entails target incubation with a randomized nucleic acid library, partitioning of bound from unbound sequences, and amplification of retained sequences for iterative enrichment (created by Bio Render).

1.1.1.1 Capillary Electrophoresis SELEX(CE-SELEX)

Capillary electrophoresis–based SELEX (CE-SELEX) enhances selection performance by exploiting differences in electrophoretic behavior between free oligonucleotides and those engaged in target binding. When an aptamer associates with its target, the resulting complex migrates through the capillary at a measurably different velocity, enabling effective physical separation without the need for immobilization. This highly discriminative partitioning step can substantially accelerate enrichment, in some cases reducing the selection process to only a few iterative cycles. Extensions of this approach, such as non-equilibrium capillary electrophoresis of equilibrium mixtures (NECEEM), further integrate kinetic analysis into the selection workflow by allowing estimation of binding affinity and dissociation rates during enrichment. Despite these

advantages, CE-based strategies remain constrained by the limited sample volume compatible with capillary injection, which can restrict the diversity of sequences screened and may influence the likelihood of identifying rare, high-affinity binders[13, 14].

1.1.1.2 Magnetic Bead-based SELEX

Magnetic bead–based SELEX relies on anchoring the target of interest to magnetically responsive supports, which are subsequently exposed to a diverse oligonucleotide library. Following the binding step, application of an external magnetic field enables rapid physical isolation of bead-associated sequences from unbound oligonucleotides remaining in solution. Variants such as FluMag-SELEX introduce fluorescently tagged primers, allowing enrichment of the selected pool to be tracked across iterative selection cycles. While this platform offers considerable experimental flexibility and has been successfully applied to a broad range of targets, including proteins and low-molecular-weight compounds, its performance is inherently influenced by target immobilization, which may alter native binding epitopes and thus affect selection outcomes[13].

1.1.1.3 Capture-SELEX

Capture-SELEX represents a targeted adaptation of bead-based selection strategies intended to address challenges associated with immobilizing low-molecular-weight targets. Rather than tethering the target to a solid support, this method anchors the oligonucleotide library to magnetic beads through hybridization with complementary, predesigned sequences. Upon exposure to the target in solution, only those sequences that experience a binding-induced structural rearrangement are displaced from the bead surface and subsequently recovered. By directly selecting for binding-coupled conformational changes, Capture-SELEX is particularly well suited for generating structure-responsive aptamers, a feature that is advantageous for signal-transduction mechanisms

in biosensing platforms. Nevertheless, the reliance on predefined hybridization domains introduces design constraints that must be carefully optimized to avoid biasing the selection toward specific folding behaviors[13, 15].

1.1.1.4 Cell -SELEX

Cell-SELEX uses whole living cells as the target, allowing for the selection of aptamers that recognize proteins in their native conformation and environment. This method is unique because it does not require prior knowledge of the specific molecular target on the cell surface, making it an excellent tool for biomarker discovery. The process involves alternating between positive selection with target cells and counter-selection with non-target cells to ensure high specificity. While highly effective for medical applications like cancer diagnosis, it often requires more cycles (up to 35) than other SELEX variants[13, 14].

1.1.2 Applications of Aptamers

Aptamer technology addresses a significant science gap by enabling high-resolution, real-time monitoring of physiological changes. Traditional clinical diagnostics often rely on single-point, invasive sampling (like venous blood draws), which cannot capture transient fluctuations in biomarkers. Aptamer-based wearable sensors fill this gap by providing a stable, non-invasive, and reproducible platform for continuous in situ analysis. Additionally, a gap exists between the discovery of sequences and their successful application due to false-positive results; modern science addresses this through rigorous characterization (such as truncation and mutation studies) to ensure these sequences are true binders before they are used in biosensor design. Furthermore, the application of Machine Learning (ML) to aptamer technology allows researchers to intelligently navigate the nearly infinite theoretical sequence space that physical laboratory

methods cannot fully explore[16-18]. DNA aptamers show strong binding affinity and exceptional specificity towards a wide range of targets, including small molecules, proteins, whole cells, and even tissues[19-21]. These features make aptamers highly effective molecular recognition elements that can match or even outperform traditional biomolecules such as antibodies. Their multifunctionality has supported the development of aptamer-based systems in analytical and diagnostic sciences, where precise target detection is required. Moreover, the stability and adaptability of aptamers have enabled their integration into biosensor design, therapeutic delivery systems, and other biomedical applications[6, 22-25]. For instance, a 21-mer ampicillin (AMP) aptamer and its complementary strand (CS) were used for the detection of ampicillin by using a turn-off fluorescent method based on PTCDI (perylenetetracarboxylic acid diimide) and gold nanoparticles (AuNPs). The presence of AMP causes the CS to dissociate from the aptamer-modified AuNPs, which then quenches the fluorescence of the PTCDI fluorophore. This developed aptasensor provides a high sensitivity with an LOD of 29.2 pM and a linear detection range of 100 pM to 1000 pM[24]. C Feng. et al. discuss various works where specific aptamers were used for the detection of small biomolecules (such as ATP, adenosine, and cocaine) using optical transduction methods including fluorescence, colorimetry, and chemiluminescence. A highlighted fluorescence aptasensor for ATP utilized graphene-based quenching and nuclease recycling to provide an LOD of 40 nmol/L[26]. Several biophysical and analytical methods (e.g., surface plasmon resonance (SPR), flow cytometry and bio-layer interferometry (BLI), etc.) are currently used to determine binding affinities, with apparent dissociation constants (K_D values) typically ranging from the nanomolar to the picomolar range for their respective targets[27-29]. Among the available techniques, BLI has emerged as especially well-suited for aptamer studies due to its ability to quantify both association and dissociation kinetics without the need for molecular labeling[30, 31]. Despite the

growing number of reported aptamer-based sensing platforms, translating these systems into reliable analytical tools for complex biological samples remains challenging[3]. In practical applications, biosensors must operate in environments rich in proteins, lipids, and other interfering species, which can promote non-specific adsorption and biofouling at the sensor interface[32, 33]. These effects can reduce selectivity and sensitivity, leading to false-positive or false-negative signals and limiting reproducibility. Consequently, there is a critical need for analytical approaches that enable systematic evaluation of aptamer binding performance, including affinity, selectivity, and resistance to non-specific interactions, under well-controlled and label-free conditions. Addressing these challenges is essential for advancing aptamer-based biosensors toward clinically and biologically relevant applications.

1.2 Bio-layer Interferometry

Biolayer interferometry (BLI) is an optical biosensing methods that uses a dip-and-read format to evaluate biomolecular interactions under real-time, label-free conditions. This technology is particularly valuable because it not only allows detailed kinetic characterization of binding events but also enables analyte detection and quantitative analysis. The system is highly flexible, which makes it suitable for both medium- and high-throughput experimental designs[34]. In addition to providing kinetic constants, BLI is particularly useful during biosensor development because it allows rapid screening of immobilization chemistries, ligand densities, and assay buffers in a microplate-based workflow. This capability is important when evaluating aptamer-based recognition in settings where non-specific adsorption and matrix effects can distort binding signals. Accordingly, BLI offers an efficient platform to quantify binding performance (affinity and kinetics) while also enabling systematic assessment of assay robustness through appropriate controls and reference subtraction[31, 35].

1.2.1 BLI principle

Biolayer interferometry (BLI) functions based on the principle of optical interference created by white light reflected from two different surfaces: an internal reference layer and a layer of biomolecules immobilized on the sensor tip. When analytes in solution interact with the immobilized ligand, the effective thickness of the biomolecular layer changes in proportion to the size and affinity of the bound molecules. This change modifies the interference pattern, resulting in producing a wavelength shift that is continuously monitored in real time. A typical BLI experiment is composed of sequential steps including baseline acquisition (buffer), association (analyte binding), and dissociation (analyte release), which together generate a sensorgram[36]. When experiments are conducted across a concentration series, the association and dissociation phases can be fit using appropriate binding models to extract kinetic rate constants (k_{on} and k_{off}) and an apparent dissociation constant (K_D)[35]. This kinetic information is valuable for comparing aptamer candidates and identifying conditions that preserve specific binding behavior. A key benefit of BLI is related to its versatility: it can monitor interactions across a wide range of targets, from small molecules and peptides to proteins, nucleic acids, and even viral particles. This broad capability has made BLI as a robust tool across many areas of biomedical research[37, 38].

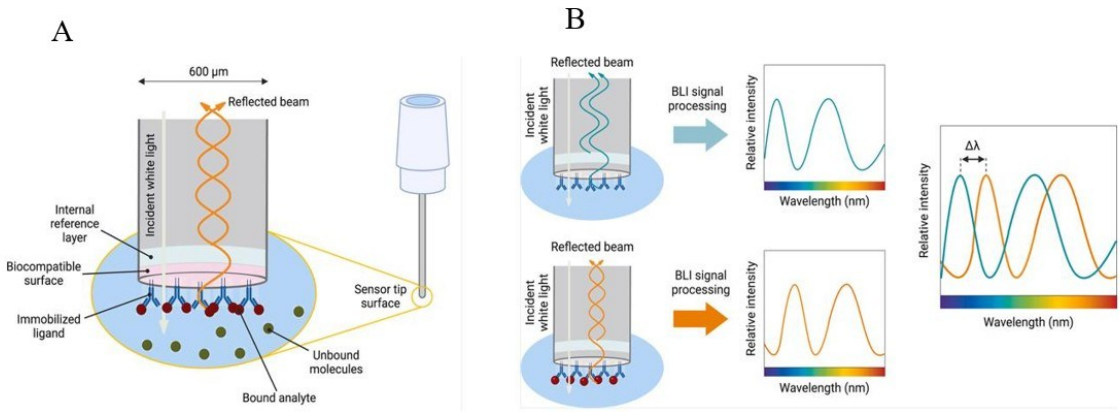

*Figure 3. (A) Illustrative representation of a biolayer interferometry (BLI) biosensor. (B) BLI signal output. Analyte binding to the sensor tip ligand is monitored as a shift in wavelength (Δλ). Reprinted from A. Jug, T. Bratkovič, J. Ilaš, TrAC Trends Anal.*Chem. *2024, 176, 11774, under the Creative Commons (CC BY 4.0) license* [31].

For biosensing applications, a critical challenge is distinguishing true target binding from non-specific interactions that arise from the sensor surface, immobilization chemistry, or sample matrix components. Such non-specific binding and surface fouling can increase baseline drift and generate apparent wavelength shifts that may be misinterpreted as positive signals (false positives). Conversely, false negatives can occur when target binding is masked by steric effects, insufficient ligand accessibility, or competitive adsorption of matrix components. Therefore, rigorous assay design in BLI commonly includes negative controls (e.g., scrambled sequences or non-binding ligands), reference sensors, and buffer additives or blocking strategies to reduce non-specific adsorption. Incorporating these controls is essential to accurately assess selectivity and to interpret binding results in complex samples[31, 39]. In this thesis, these considerations are particularly important because the studied targets (protein biomarkers, extracellular vesicles, and viral particles) represent increasingly complex analytes for which selectivity and resistance to non-specific interactions are key determinants of analytical performance.

1.3 KI-67 Protein

Ki-67, also known as the Marker of Proliferation Ki-67 (MKI67), is a nuclear protein expressed in human cells. Its presence is limited to the active phases of the cell cycle, namely G1, S, G2, and mitosis. It is absent in quiescent cells in the G0 phase[40]. Since its discovery in 1983[41], both its expression dynamics and subcellular localization across the cell cycle have been extensively investigated. The protein is encoded by the MKI67 gene and is characterized by several conserved structural domains. The N-terminal region of Ki-67 contains a forkhead-associated (FHA) domain, a structural motif that specifically binds phosphorylated protein epitopes. Through this domain, Ki-67 interacts with specific phosphoproteins during mitosis[42, 43]. In addition, all Ki-67 homologs possess a conserved protein phosphatase 1 (PP1) interaction motif[44]. The PP1 family, which consists of three isoforms (α, β, and γ), is estimated to mediate nearly one-third of protein dephosphorylation events in eukaryotic cells, showing its central role in diverse cellular processes[45]. The central portion of Ki-67 is composed of tandem repeat sequences, several of which undergo phosphorylation during mitosis[46]. On the surface of mitotic chromosomes, the strong positive charge of Ki-67 acts as an electrostatic barrier that minimizes excessive aggregation of chromosome arms[47, 48]. Localization of Ki-67 within the cell is determined by its intrinsically disordered regions[49]: the conserved domain (CD) directs nucleolar localization, whereas the leucine/arginine-rich (LR) domain located at the C-terminus mediates binding to heterochromatin during interphase and association with the chromosome periphery in mitosis. This LR domain directly interacts with DNA, and its binding affinity is reduced upon phosphorylation[50, 51].

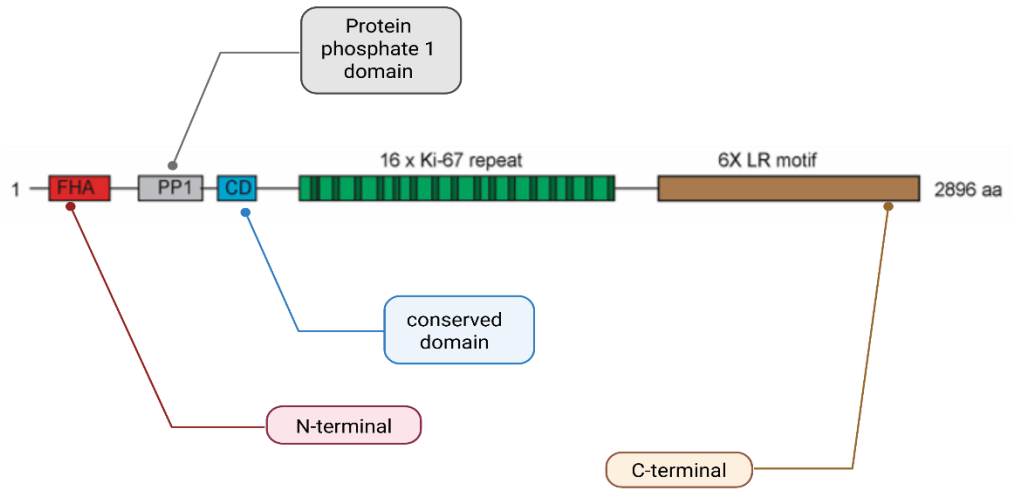

Figure 4.A schematic diagram of human Ki-67 structure (Adapted with permission from Springer Nature).

Ki-67 is active in both interphase and mitotic cells, and its location inside the cell changes a lot depending on the stage of the cell cycle. These spatial differences are linked to different cellular roles. In interphase, Ki-67 is essential for maintaining the proper organization and distribution of heterochromatin-associated antigens[52-54]. During mitosis, it contributes to the formation of the perichromosomal layer, a ribonucleoprotein sheath surrounding condensed chromosomes, that prevents chromosome aggregation and facilitates accurate segregation[55, 56]. In addition to these structural contributions, Ki-67 interacts with various nuclear proteins to influence chromatin organization, transcriptional control, and mitotic regulation, and it may also contribute to phase separation within nuclear subdomains. Although it does not act as a transcription factor[57, 58], Ki-67 indirectly influences gene expression by altering chromatin accessibility and nuclear architecture. This regulatory capacity contributes to cellular adaptability and, in malignant contexts, supports the maintenance of hybrid EMT-state phenotypes. Consequently, Ki-67 plays a

key role in oncogenic transformation, tumor progression, metastatic dissemination, and immune responses against tumors. Importantly, its expression level reflects the growth fraction of cell populations, which has made it as a widely used indicator of proliferative activity in both normal and pathological tissues. Elevated Ki-67 expression in cancer specimens is frequently associated with aggressive behavior and rapid expansion, highlighting its clinical value as a prognostic biomarker[59]. Despite its widespread use as a proliferation marker, accurate detection of Ki-67 presents several analytical challenges. Ki-67 is a large, intrinsically disordered nuclear protein whose expression level and subcellular localization vary dynamically throughout the cell cycle. These features complicate selective detection, particularly in heterogeneous biological samples where Ki-67 abundance may be low or spatially restricted. Furthermore, conformational flexibility and epitope accessibility can influence binding interactions, increasing the risk of false-negative signals when recognition elements fail to access relevant binding regions[60]. Clinically, Ki-67 expression is most commonly evaluated using antibody-based immunohistochemical or immunofluorescence assays. While these methods are well established, they are largely qualitative or semi-quantitative and are sensitive to antibody specificity, epitope masking, and experimental conditions. Variability in antibody performance and sample preparation can contribute to inconsistent results and inter-observer variability, underscoring the need for alternative analytical approaches capable of providing quantitative and reproducible measurements of Ki-67 binding interactions[61].

From an analytical perspective, Ki-67 represents a challenging but informative target for biosensor development due to its size, structural disorder, and context-dependent accessibility. These characteristics make Ki-67 an ideal model system for evaluating the performance of alternative recognition strategies, such as aptamer-based sensing, in comparison to conventional antibody

approaches. When coupled with label-free techniques like bio-layer interferometry, aptamer-based assays enable quantitative assessment of binding affinity, kinetics, and selectivity, while allowing systematic evaluation of non-specific interactions and assay robustness. As such, Ki-67 provides a relevant biological target for investigating the strengths and limitations of aptamer-based biosensing platforms[35].

1.4 Exosomes

The term "exosomes" was first introduced by Trams et al. and Heine, who defined them as extracellular vesicles detached from the surface of the cell[62, 63]. Exosomes are macrovesicles of typically 30-150 nm diameter and are typically characterized as enriched for selective protein markers including tetraspanin (CD63, CD81, CD9), heat shock protein 70 (HSP70), Tsg101, and ALIX[64, 65]. Their biogenesis is outlined in Figure 5. Briefly, Exosomes are derived as intraluminal vesicles (ILVs) within endosomes[66]. In the late phase of endosomal maturation, the compartments are called multivesicular bodies (MVBs). Protein and cargo on the MVB limiting membrane condense into microdomains with the aid of ESCRT structures or independently. ILV scission, partially mediated through ESCRT-III, creates macrovesicles of low size within the MVB[67]. Upon fusing with the plasma membrane, ILVs are extruded to the extracellular milieu as exosomes. This event was first imaged using electron microscopy in 1985 by Pan et al[68]. Exosomes are responsible for intercellular information transfer, transferring DNA, RNA, proteins, and metabolites across cells[64, 65]. In breast malignancy, cargo within them may include information, providing molecules capable of inducing metastatic and proliferation pathways[65]. Additionally, since exosomes are found in readily accessible body fluids, including blood and urine, they represent an important prospect for a non-invasive disease marker. Therefore, some proven surface protein markers,

including MUC1, 5TR1, and CD63, will be used for detecting breast cancer-derived exosomes[69-71].

Despite their diagnostic potential, exosomes are analytically challenging targets due to their nanoscale size, heterogeneous composition, and overlap with other extracellular vesicle populations. Exosomes coexist with microvesicles, apoptotic bodies, and protein aggregates in biological fluids, making selective detection difficult. In addition, exosome concentration and surface marker expression can vary significantly depending on cell type, physiological state, and isolation method, complicating quantitative analysis. Although tetraspanins such as CD63, CD81, and CD9 are commonly used as exosome markers, they are not exclusively expressed on tumor-derived vesicles and may also be present on vesicles released from healthy cells. As a result, marker-based detection strategies can generate false-positive signals when non-malignant extracellular vesicles are captured. Conversely, false-negative results may occur when target vesicles express low levels of a selected marker or when epitope accessibility is reduced due to vesicle orientation or surface crowding. These limitations highlight the importance of evaluating

selectivity and marker performance when developing exosome detection assays[72].

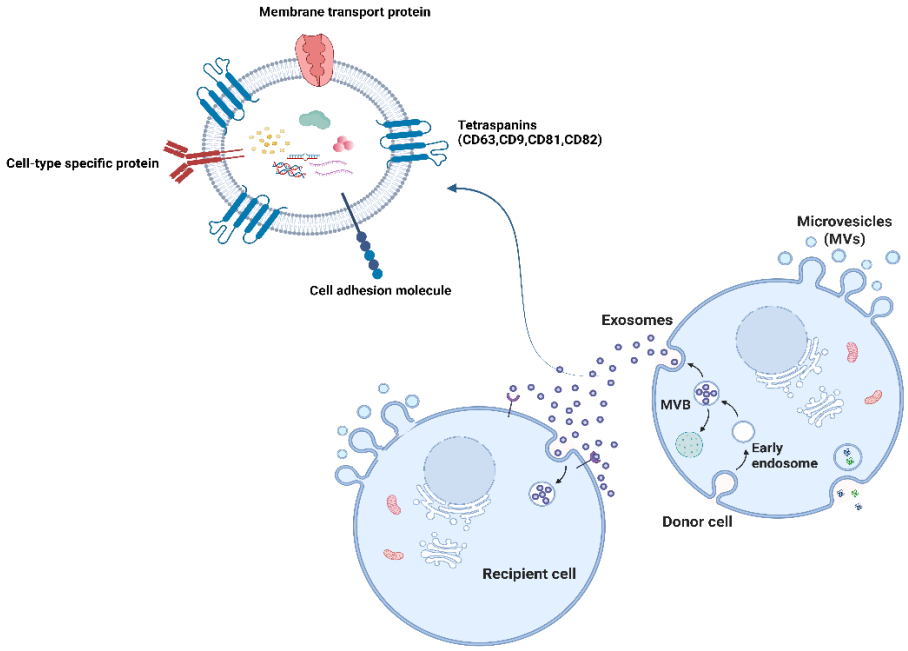

Figure 5.Overview of exosome production pathway (created by Bio Render).

From an analytical perspective, exosomes represent complex and biologically relevant targets that challenge the selectivity and robustness of biosensing platforms. Their nanoscale size, heterogeneous surface composition, and presence in protein-rich biological matrices make them particularly susceptible to non-specific adsorption and biofouling effects in surface-based assays. Consequently, there is a need for sensing strategies that enable quantitative and label-free evaluation of binding interactions while incorporating appropriate controls to distinguish specific vesicle capture from background signals[73]. In this thesis, aptamer-based recognition elements combined with bio-layer interferometry are employed to systematically assess binding behavior, selectivity, and non-specific interactions in exosome detection.

1.5 SARS-CoV-2 pseudoviruses

After the emergence of a novel coronavirus in late 2019, later named severe acute respiratory syndrome coronavirus 2 (SARS-CoV-2), cases of Coronavirus Disease 2019 (COVID-19) rapidly increased worldwide, resulting in a global pandemic[74]. SARS-CoV-2 is a positive, single-stranded RNA virus belonging to the Betacoronavirus genus of the Coronaviridae family. Its structure is defined by several key proteins encoded by the viral genome, including the nucleocapsid (N), spike glycoprotein (S), envelope (E), and membrane (M) proteins(Figure 6)[75, 76]. Among these, the spike glycoprotein is the biggest transmembrane protein and plays a central role in viral entry. The spike is composed of two functional subunits: S1, which contains the receptor-binding domain (RBD) that binds with high affinity to the human angiotensin-converting enzyme 2 (ACE2) receptor, and S2, which promotes membrane fusion, which allows incorporation of viral components into the host cell[77]. Because the spike protein is the primary mediator of SARS-CoV-2 entry through its receptor-binding domain (RBD) and fusion machinery (Figure 6), it has become the central target in diagnostics, vaccine design, and therapeutic strategies. This critical role of the spike protein also supports the development of SARS-CoV-2 pseudoviruses. The pseudovirus system is built specifically to mimic the spike protein's role in the viral entry mechanism but can be handled under lower biosafety conditions, making it a practical and safe target for analytical approaches. Pseudovirus systems provide a practical and analytically relevant model for studying viral surface recognition while avoiding the biosafety constraints associated with live pathogenic viruses. By presenting the viral spike protein in a membrane context that closely mimics native virions, pseudoviruses preserve key structural and functional features required for binding interactions. As a result, pseudoviruses are widely used for evaluating binding, neutralization, and sensing

strategies targeting viral entry mechanisms under controlled laboratory conditions. From an analytical perspective, intact viral particles present challenging targets for biosensing due to their nanoscale size, multivalent surface architecture, and dependence on conformationally intact surface proteins for recognition. Viral detection assays must discriminate specific binding to viral antigens from non-specific interactions with host-derived proteins, vesicles, or debris present in complex samples. These challenges can lead to false-positive signals arising from non-specific adsorption or cross-reactivity, as well as false-negative results when surface epitopes are partially masked or structurally altered[78].

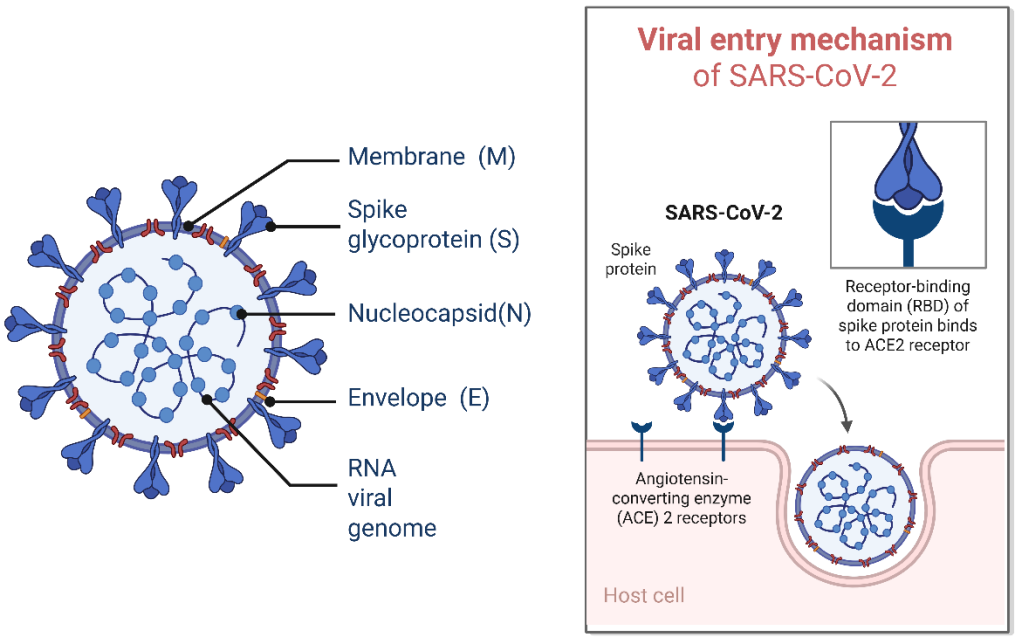

Figure 6. SARS-COV-2 Structure and viral entry mechanism (created by Bio Render).

From a biosensing standpoint, SARS-CoV-2 pseudoviruses represent complex, multivalent targets that are well suited for evaluating the performance of surface-based, label-free analytical platforms. Their size and surface protein organization make them particularly sensitive to assay selectivity, non-specific adsorption, and surface fouling effects. Consequently, the use of aptamer-based recognition elements in combination with bio-layer interferometry enables quantitative assessment of binding affinity, kinetics, and specificity while incorporating appropriate negative controls to minimize false signal interpretation. This system therefore provides a relevant model for assessing aptamer-based sensing strategies for viral targets.

1.6 Rationale and Thesis Objective

Detecting disease biomarkers early and accurately is very important for diagnosis and treatment. Traditional methods like antibody-based tests are often expensive, time-consuming, and sometimes give variable results. Despite significant advances in biosensing technologies, many existing platforms lack a unified analytical framework capable of systematically evaluating binding affinity, selectivity, and non-specific interactions across different classes of biological targets. In complex biological environments, non-specific adsorption and surface fouling can lead to false-positive signals, while limited epitope accessibility or weak binding can result in false-negative outcomes. These challenges highlight a critical gap between proof-of-concept sensing approaches and robust analytical methods suitable for reliable biomarker detection. Because of that, there is a need for a simpler and more reliable method. Aptamers offer advantages such as chemical stability, reproducible synthesis, and tunable surface immobilization, which make them well suited for integration with surface-based, label-free techniques. Bio-layer interferometry enables real-time monitoring of association and dissociation processes, allowing quantitative

comparison of binding kinetics while incorporating appropriate reference controls to assess non-specific binding. Together, aptamers and BLI provide a rational platform for addressing selectivity limitations and improving analytical confidence in biomolecular interaction studies. Using aptamers with BLI makes detection faster, cheaper, and more stable, which can be very useful in studying cancer and viral biomarkers. The main goal of this thesis was to develop and test aptamer-based BLI sensors for detecting different biological targets related to cancer and viral infection. The first goal was to study the binding between a DNA aptamer and the Ki-67 protein, which is a well-known marker of cell growth. The second goal was to design a BLI system using CD63, MUC1, and 5TR1 aptamers to detect breast cancer-derived exosomes. The third goal was to apply this approach to detect SARS-CoV-2 pseudoviruses using new aptamers that can recognize the spike protein. Collectively, these three objectives were designed to evaluate the performance of aptamer-based BLI sensing across increasingly complex biological targets, ranging from soluble proteins to extracellular vesicles and virus-like particles, thereby assessing the versatility, selectivity, and robustness of this analytical approach.

Chapter 2

Biolayer Interferometry (BLI) Validation of KI-67 Aptamer

2 Abstract

Ki-67 is a nuclear protein widely used as an indicator of cell proliferation in cancer diagnostics; however, its functional role is increasingly recognized to involve dynamic molecular interactions rather than static expression alone. In particular, the C-terminal region of Ki-67 is enriched in basic residues and intrinsically disordered segments, suggesting that its functional role is closely linked to dynamic binding interactions rather than static expression alone. Traditional antibody-based assays used to study Ki-67 are primarily optimized for endpoint detection and localization, limiting their ability to provide quantitative insight into binding strength, kinetics, and selectivity. In this study, an aptamer-based biolayer interferometry (BLI) platform was employed to quantitatively investigate the binding characteristics of a recombinant Ki-67 under controlled conditions. The use of BLI enabled real-time, label-free monitoring of interaction kinetics and affinity, providing mechanistic insight beyond simple detection. The selected Ki-67 aptamer exhibited a dissociation constant of 10.9 ± 0.6 nM and showed a linear binding response across the tested concentration range, with a limit of detection of 29.0 nM and a limit of quantification of 87.5 nM. Binding

selectivity was assessed using a scrambled oligonucleotide control in the presence of tRNA to suppress non-specific electrostatic interactions. Although the scrambled sequence displayed residual binding, consistent with the positively charged nature of the Ki-67 C-terminal domain, its weaker affinity ($K_D = 35 \pm 16$ nM) indicated preferential binding of the selected aptamer. Together, these results demonstrate that aptamer-based BLI provides a quantitative and informative platform for evaluating Ki-67 binding behavior and supports the use of aptamers as suitable recognition elements for studying highly charged proliferation-associated proteins.

2.1 Introduction

Ki-67 is best known as a marker used to assess cell proliferation in cancer, yet growing research indicates that its role within the cell is more complex than simply signaling whether a cell is dividing. The protein contains large flexible regions and a strongly positively charged segment at its C-terminus, structural features that support transient interactions with nucleic acids and play a role in organizing chromosomes throughout the cell cycle. These characteristics suggest that Ki-67 function is governed not only by how much of the protein is present, but also by how it interacts with other molecular components. For this reason, examining the binding behavior of Ki-67 in well-defined experimental systems is important for understanding both its biological activity and its analytical response in molecular assays[60]. Although Ki-67 plays an important role in cell biology, its binding behavior has proven challenging to study with standard analytical tools. Much of the existing research relies on antibody-based methods that are well suited for detecting and visualizing the protein but offer little insight into how strongly or dynamically it interacts with other molecules. In addition, the pronounced positive charge of Ki-67, especially within its C-terminal region, makes results from affinity-based assays difficult to interpret, as electrostatic attraction and multiple weak interactions can contribute to the observed signal[51]. Techniques aimed

at structural characterization face further obstacles, since the large size and flexible nature of Ki-67 limit their usefulness for routine and quantitative binding studies[79]. Given these challenges, investigating the binding behavior of Ki-67 calls for a method that can capture interaction dynamics while recognizing that a certain level of non-specific electrostatic attraction is inherent to the protein. Instead of attempting to remove all background interactions, an effective analytical approach should make it possible to measure these contributions and separate them from more selective binding effects. The aptamer-based biolayer interferometry strategy applied in this study meets these needs by providing real-time, label-free monitoring of interactions under controlled experimental conditions and enabling direct comparison with carefully designed control sequences. In addition to measuring binding affinity, BLI enables analysis of association and dissociation kinetics while incorporating reference sensors and negative controls to assess non-specific binding. These features make BLI an appropriate tool for validating the performance of aptamer-based recognition elements prior to their application in more complex sensing formats. Within this framework, binding selectivity can be assessed quantitatively, even when low-level interactions with non-specific nucleic acids are anticipated due to the protein's charged nature[80, 81]. In line with this rationale, the present chapter examines the binding behavior of Ki-67 using an aptamer-based biolayer interferometry platform, with particular attention to binding strength, relative selectivity, and the role of electrostatic interactions. By emphasizing kinetic measurements and the use of well-defined control strategies, this approach enables a level of insight into Ki-67 interactions that is difficult to achieve with conventional, detection-oriented methods and provides a structured framework for assessing the protein's potential as a biosensing target.

2.2 Materials and Methods

The Ki-67 aptamer was selected by Dr. Anya Kichkailo and her team from Krasnoyarsk State Medical University, Russia (5'CCACGGTCCGTGCTAGGGAATGTACACACGGTGCGTCGTCCATTGGCATA-3') and the scrambled sequence (5'GTGCCTCGGACAAGCAACCGTGAGGTATGTACCGCGTTCGACCATGGTCT-3') were purchased from IDT DNA Technology (Iowa, USA) by a custom order. The Ki-67 protein (AA 3120-3256) (His-tag) was purchased from ANTIBODIES ONLINE (Limerick, PA United States). BSA (Cat. No. A9418), Tween 20 (Cat. No. 9005-64-5),

Phosphate buffer saline (PBS) without Ca^{2+}-Mg^{2+} (Cat. No. 10010031) and DPBS with Ca^{2+}-Mg^{2+} (Cat. No. 14040141) were purchased from Gibco. tRNA (Cat. No. 15401-011) was purchased from Thermo Fisher Scientific. All buffers should be filtered through a 0.22 µm filter before use.

2.2.1 BLI-Based Screening of DNA Aptamer Affinity to Ki-67 protein

We employed Ni-NTA biosensors and a BLI apparatus called Octet N1 (Sartorius, Bohemia, NY) to characterize the binding affinity of the Ki-67 aptamer and the Ki-67 protein. Firstly, the aptamer was prepared in the assay buffer (DPBS with 1mM $CaCl_2$, 0.5mM $MgCl_2$,0.02% BSA and 0.05% Tween20 pH 7.4) at the serial dilutions of 400, 200, 100, and 50 nM, and after heating up at 95°C for 5 minutes, they were cooled on ice for 10 minutes. Prior to assay, the Ni-NTA biosensors were pre-hydrated in assay buffer for 10 minutes. The binding assay was performed in 0.5 mL light-blocking tubes at 25°C with a total volume of 250 µL. The assay (Figure 7) initiated with a baseline step of 30 seconds in the optimum assay buffer. Then, 20 µg/mL of his-tagged Ki-67 protein was immobilized on the Ni-NTA biosensor tips for 90 s. The second baseline was performed for 30 seconds prior to the association with 130 seconds in which different concentrations of Ki-67 aptamer were loaded and dissociated in the next step within 130 seconds.

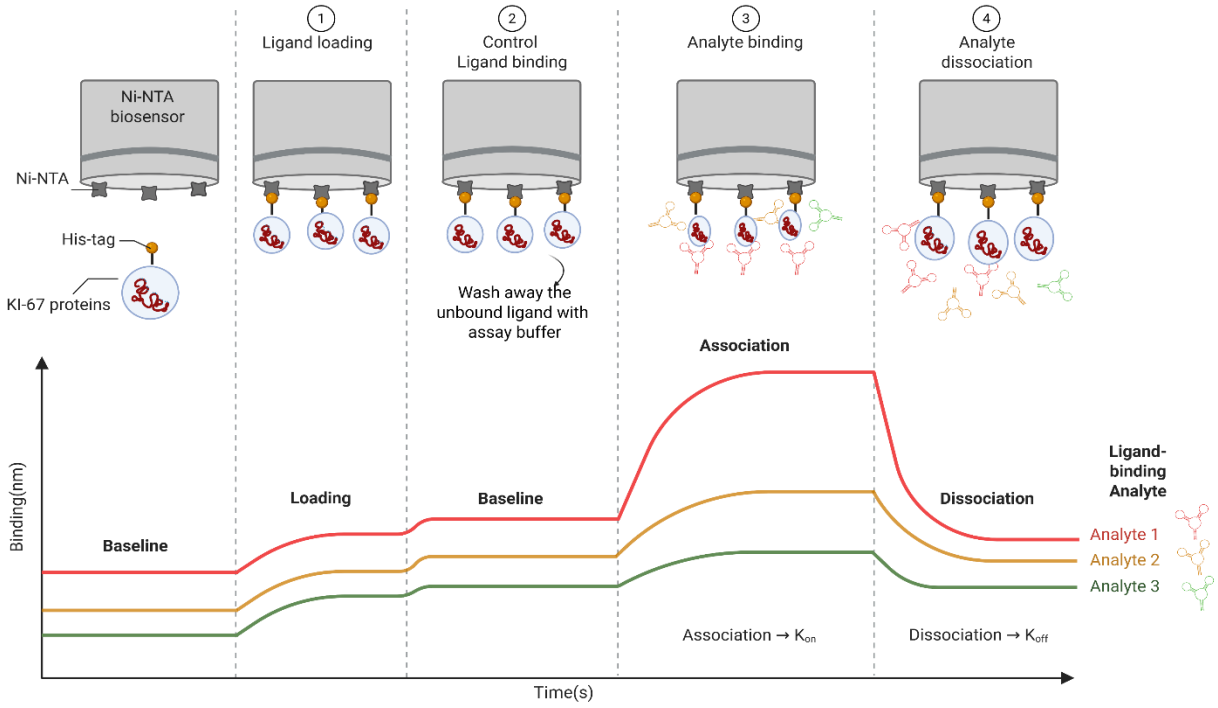

Figure 7.Schematic BLI workflow of aptamer-protein affinity test (created by Bio Render).

2.2.2 Specificity assessment of Ki-67 protein using scrambled sequence

In the specificity analysis, the scramble sequence was prepared as in the previous section. In short, 400 nM of aptamer was prepared in assay buffer, heated to 95°C for 5 minutes, and then cooled on ice for 10 minutes. Then, a series of tRNA dilutions (0.1, 0.01, 0.001, and 0.0001 ng/µl) was added to the scrambled sequence and incubated for 30 minutes.

2.3 Results

2.3.1 Binding evaluation and K_D determination of aptamer to Ki-67 protein

The his-tagged Ki-67 protein was loaded onto a Ni-NTA biosensor, and various concentrations of the Ki-67 aptamer were prepared in optimum assay buffer to assess binding to the Ki-67 protein (Figure 8). In this configuration, His-tagged Ki-67 protein was immobilized on Ni-NTA biosensors, while the aptamer was introduced as the soluble analyte. This orientation ensured that the measured signal reflected aptamer-protein binding rather than aptamer surface immobilization effects. Control sensors without immobilized protein were included to account for baseline drift and non-specific adsorption to the sensor surface. The binding measurement took place within 14 minutes per sample. The binding shifts on the aptamer-based BLI during the interaction with the Ki-67 protein indicated a dose-dependent response. As a result, the Ki-67 protein could bind the aptamer within a concentration range of 400 to 50 nM, and the control assay was prepared in the absence of the aptamer. The K_D value of 10.9 ± 0.6 nM was obtained from kinetic analysis based on the default 1:1 binding model in the Octet N1 software.

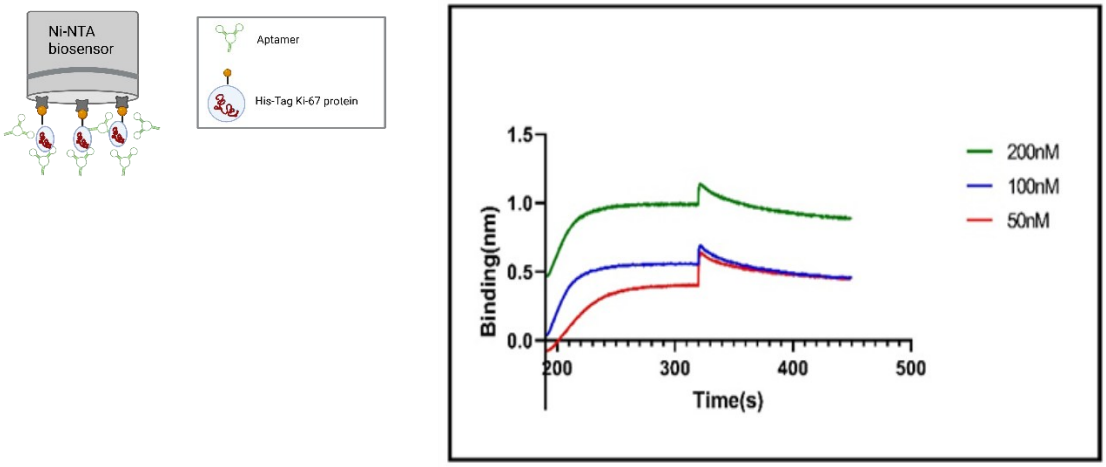

Figure 8.Real-time detection of Ki-67 protein.

2.3.2 Determination of quantitative binding parameters

To estimate the quantitative parameters, including Limit of detection (LOD) and Limit of quantification (LOQ) a calibration curve was built by plotting the BLI response versus KI-67 aptamer concentration. Calibration plot showing the correlation between Ki-67 protein and aptamer binding response measured by Biolayer Interferometry. A strong linear correlation (R^2 = 0.9653) described by the regression equation Y = 0.0045X + 0.1187. Error bars indicate the standard deviation from three independent replicates (n = 3). The response is linear across my working range 50–400 nM (Figure 9). The LOD and LOQ through linear equation were found to be 29.0 nM and 87.5 nM respectively.

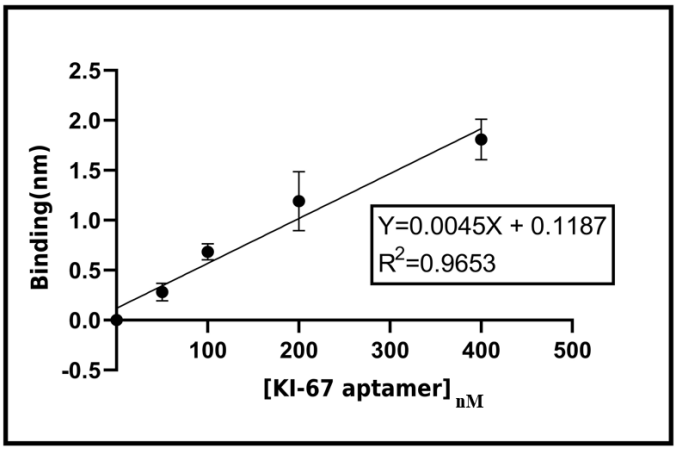

Figure 9.Linear calibration curve of Ki-67 aptamer.

2.3.3 Specificity assay of aptamer binding to Ki-67 protein

To verify the selectivity of the Ki-67 protein to the corresponding aptamer, its binding affinity was tested against a scrambled sequence. For this purpose, first, tRNA was titrated in the range of 0 to 0.1ng/µl to find the optimum concentration of it. Transfer RNA (tRNA) was employed as a polyanionic blocking agent to suppress non-specific electrostatic interactions between nucleic acids and the Ki-67 protein, particularly interactions arising from charge-based attraction rather than sequence- or structure-dependent recognition. The optimized tRNA concentration was selected to minimize scrambled-sequence binding while preserving a measurable signal for the Ki-67 aptamer. The Ki-67 aptamer was considered as a control assay. As the tRNA concentration increased, both signals dropped, but the scrambled one dropped more (Figure 10). To minimize nonspecific binding from the scrambled while preserving a strong aptamer signal, I used the minimal dose (0.001 ng).

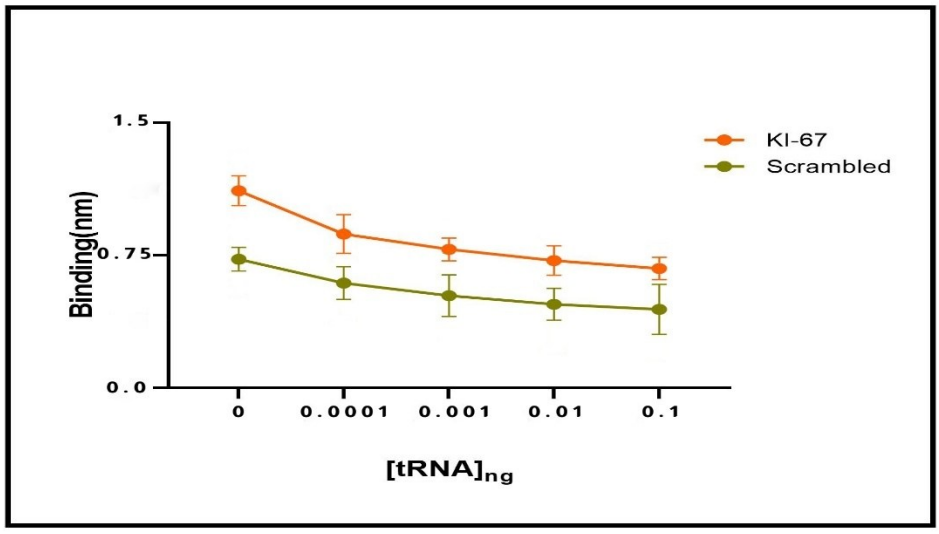

Figure 10.Determining the optimal tRNA concentration for reducing non-specific interactions.

Under the optimized experimental conditions, the selectivity of the Ki-67 aptamer was assessed by directly comparing its binding profile with that of a scrambled oligonucleotide (Figure 11). By comparing the binding of the Ki-67 aptamer vs the scrambled sequence, the scrambled sequence generated a measurable but noticeably weaker binding response than the Ki-67 aptamer. This low-level signal is consistent with non-specific electrostatic attraction between the negatively charged nucleic acid backbone and the positively charged regions of the Ki-67 C-terminal domain. Analysis of the binding data yielded a dissociation constant of 10.9 ± 0.6 nM for the Ki-67 aptamer, whereas the scrambled sequence exhibited a substantially weaker interaction with a K_D of 35 ± 16 nM, representing an approximate three-fold difference in affinity. Although the scrambled sequence binding reflects an inherent electrostatic component of Ki-67 interactions, the stronger affinity observed for the selected aptamer points to the involvement of additional sequence- and structure-dependent recognition mechanisms. Both interactions were measured under the same experimental conditions, including the use of detergent, blocking proteins, and competitor nucleic acids, to reduce non-specific adsorption. Within this controlled setting, the consistently higher binding response of the Ki-67 aptamer compared to the scrambled control supports preferential interaction that cannot be explained by charge effects alone. Taken together, these findings suggest that while Ki-67 displays a general tendency to associate with nucleic acids, the selected aptamer engages the protein through a more defined and selective binding mode, supporting its suitability for probing Ki-67 binding behavior.

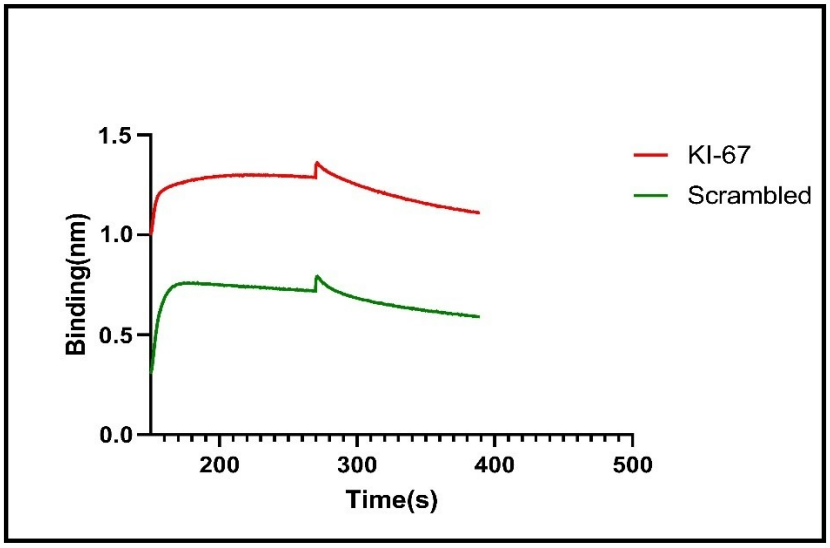

Figure 11. Evaluation of specific binding of Ki-67 protein toward the Ki-67 aptamer.

2.4 Discussion

Ki-67 is a nuclear protein found solely in proliferating cells and absent in the resting (G_0) phases, making it one of the most reliable indicators for cellular proliferation and tumor grading[41, 82]. Due to its expression level being directly proportional to the growth fraction of a specific cell type, Ki-67 holds considerable diagnostic and prognostic significance in oncology, especially in breast, lung, and brain malignancies[83]. Consequently, it is imperative to detect Ki-67 with high sensitivity and specificity for the assessment of tumor aggressiveness and therapy response. However, traditional immunohistochemistry (IHC) methods are limited by artifacts from fixation, differences in antibodies, and subjective interpretation[84]. In this context, aptamer-based biosensing technologies like Biolayer Interferometry (BLI) provide a strong and label-free way to do real-time kinetic and analytical analysis. The experimental workflow was designed and optimized to obtain reproducible and reliable kinetics data. For instance, the pre-heating and snap-cooling steps prior to measurement ensured the aptamer adopted its active conformation, further contributing to

consistent response curves .The optimized assay buffer containing Ca^{2+}, Mg^{2+}, BSA, and Tween-20 minimizing hydrophobic adsorption on the biosensor tip and improved signal stability by promoting proper aptamer folding (via Mg^{2+} stabilization of G-quadruplex or hairpin structures). Through the 1:1 model of binding the K_D value was obtained with 10.9 ± 0.6 nM, signifying the strength of binding affinity between Ki-67 protein and aptamer. Also, the linear relationship between BLI response and Ki-67 concentration (R^2 = 0.9653) emphasized the strong interaction across the working range from 50–400 nM. Direct, apples-to-apples K_D reports for Ki-67 are rare in the biosensor literature, most Ki-67 sensor papers focus on analytical performance like LOD rather than molecular kinetics. Nevertheless, the nanomolar K_D can be contextualized against Ki-67 biosensors that report sensitivity. The determined limit of detection of 29.0 nM and limit of quantification of 87.5 nM indicate a high sensitivity level for an optical aptasensor operating in label-free conditions. It should be noted that the BLI assay developed here measures aptamer binding to purified Ki-67 protein under controlled conditions rather than direct detection of Ki-67 in complex biological samples. As such, the reported LOD and LOQ reflect analytical sensitivity of the binding interaction rather than clinical detection sensitivity. This distinction is important when comparing performance metrics across different sensing platforms. For comparison, An electrochemical immunosensor (AuNP–polydopamine/graphene) reported LOD of 1.7 pg mL^{-1} for purified Ki-67 with a 4–800 pg mL^{-1} linear range, demonstrating deep sub-pg sensitivity via surface amplification[85]. A flow cytometry assay to measure intracellular Ki67 expression reported LOD of 4 pg/mL with a 10 to 100 pg/mL linear range[86]. Kim et al. established a microfluidic electrochemical immunosensor for detection of Ki-67 in 3D tumor spheroids with limits of detection of 0.97 ng/mL[87]. Most published sensors are immunosensors that report mass-concentration LODs, while this work provides mechanistic binding sensitivity in the expected nM

regime for label-free readouts. Taken together, the calibration and LOD/LOQ place the BLI aptamer assay in a performance window consistent with reliable Ki-67 quantification, while highlighting the distinct advantages (kinetics, simplicity) and trade-offs (no enzymatic amplification) of label-free optical sensing. Additional confirmation of the aptamer's selectivity was conducted via considering scrambled sequence in which the optimum concentration of tRNA was applied to suppressed non-specific binding of scrambled sequence towards Ki-67 protein while preserving the specific binding of Ki-67 protein and its corresponding aptamer. As a result, scrambled sequence displayed weaker affinity with 35 ± 16 nM. The approximately three-fold difference in apparent dissociation constant between the Ki-67 aptamer and the scrambled sequence indicates preferential binding; however, this difference alone does not constitute absolute selectivity. Rather, it demonstrates that sequence and structural features of the aptamer contribute measurably to binding strength under the tested conditions. This difference showed that the observed binding is sequence dependent and not due to the nonspecific adsorption also, the specific secondary and tertiary structure of the Ki-67 aptamer is essential for target recognition. It is important to consider the intrinsic biochemical properties of Ki-67 when interpreting these results. Ki-67 contains a C-terminal arginine-rich region known to interact with DNA and chromatin, raising the possibility that part of the observed binding signal arises from non-sequence-specific electrostatic interactions with nucleic acids. Although the reduced affinity observed for the scrambled sequence suggests a contribution from aptamer structure, these data alone cannot fully exclude a component of charge-mediated binding. To more rigorously establish molecular selectivity, future studies could include competition assays using excess non-specific DNA or RNA, salt-dependence experiments to probe electrostatic contributions, and testing against unrelated nuclear or chromatin-associated proteins. In addition, evaluating aptamer binding in

complex biological matrices such as cell lysates or serum would provide insight into biofouling, matrix effects, and false-positive behavior. Such experiments would help distinguish true target-specific recognition from generalized nucleic acid–protein interactions.

Overall, these results indicate that the Ki-67 aptamer may function as a dependable probe for the detection of Ki-67 in cancer-related diagnostic investigations. The elevated affinity and specificity confirm the efficacy of the developed BLI-based platform for investigating aptamer-protein interactions.

2.5 Conclusion

This chapter demonstrated the use of an aptamer-based biolayer interferometry approach to investigate the binding behavior of the Ki-67 protein, with emphasis on affinity, relative selectivity, and the contribution of electrostatic interactions. The results showed that the selected Ki-67 aptamer binds the protein with nanomolar affinity and produces reproducible, concentration-dependent responses under optimized assay conditions. Unlike conventional antibody-based assays, which are primarily detection-oriented, the BLI platform enabled real-time kinetic analysis and quantitative comparison of binding interactions, offering insight into the molecular behavior of Ki-67 rather than solely its presence.

Selectivity assessment using a scrambled sequence revealed measurable background binding, reflecting the inherent nucleic acid affinity of the positively charged Ki-67 C-terminal region. By incorporating tRNA as a blocking agent, non-specific electrostatic interactions were reduced, allowing preferential aptamer binding to be evaluated quantitatively. The observed three-fold difference in dissociation constants between the aptamer and scrambled control indicates that sequence and structural features of the aptamer contribute meaningfully to binding strength, even

in the presence of unavoidable charge-mediated interactions. Overall, this work establishes aptamer-based BLI as a robust and appropriate platform for studying the binding behavior of Ki-67 and provides a foundation for further validation and extension of this approach to more complex biological environments.

Chapter 3

BLI Validation of Cancer Exosomes Using CD63, MUC1, and 5TR1 Aptamers

3 Abstract

Exosomes are nanoscale extracellular vesicles that carry molecular information reflective of their parental cells, making them promising targets for cancer diagnostics. However, their small size, heterogeneous surface composition, and multivalent nature pose significant challenges for selective and quantitative detection using surface-based biosensing platforms. In this chapter, an aptamer-based biolayer interferometry (BLI) platform was developed and evaluated for the detection of breast cancer–derived exosomes using three surface marker aptamers targeting CD63, MUC1, and 5TR1. Exosomes isolated from MDA-MB-231 cells were characterized by dynamic light scattering and transmission electron microscopy to confirm size, morphology, and suitability for downstream binding analysis prior to BLI measurements. Real-time BLI experiments demonstrated concentration-dependent binding of exosomes to all three cancer-associated aptamers, with CD63 exhibiting the strongest apparent affinity, followed by MUC1 and 5TR1. Binding responses were observed in the low picomolar concentration range, and calibration curves enabled estimation of limits of detection and quantification for each aptamer. A scrambled

sequence was used as a negative control and showed substantially weaker binding and faster dissociation, supporting preferential marker-dependent recognition rather than non-specific adsorption. Although the extracted dissociation constants represent apparent affinities influenced by multivalent interactions, the consistent ranking of binding strength and clear differentiation from the scrambled control validate the aptamer-BLI platform as a robust, label-free approach for assessing exosome binding behavior and marker selectivity under controlled conditions.

3.1 Introduction

Exosomes are small intracellular vesicular packets of information[64, 65]. These molecular cargos contain proteins, miRNA, RNA, and DNA, transferring between cells. These nanosized lipid vesicles are essential in both pathological and physiological processes as they can change how recipient cells work. And owing to notable properties and the crucial information they convey about their cellular origins, they have become as valuable tools in biosensing applications, particularly in cancer detection. Despite their diagnostic potential, exosomes present significant analytical challenges due to their nanoscale size, heterogeneous composition, and overlap with other extracellular vesicle populations present in biological fluids. In complex samples, non-specific adsorption, vesicle aggregation, and co-isolated proteins can contribute to false-positive signals, while variable surface marker expression can lead to false-negative outcomes. These factors make selective and quantitative exosome detection particularly challenging for surface-based biosensing platforms. In this context, aptamers can be engineered to selectively bind to exosome surface markers, facilitating the targeted identification of disease-derived exosomes. In this study, CD63 was selected as a canonical exosome marker due to its high abundance on extracellular vesicles, while MUC1 and 5TR1 were chosen as cancer-associated surface markers that are frequently overexpressed on breast cancer–derived exosomes. The combined use of a

general exosome marker and tumor-associated markers provide a strategy to evaluate both vesicle capture efficiency and disease relevance, while also enabling assessment of marker-dependent selectivity. By using Biolayer Interferometry (BLI), these aptamer-exosome interactions can be monitored in real time and label-free. Bio-layer interferometry is particularly well suited for exosome analysis because it allows real-time monitoring of surface binding events without the need for fluorescent or enzymatic labels, which can alter vesicle integrity. In addition, BLI enables evaluation of binding kinetics, assay reproducibility, and non-specific interactions through reference sensors and control sequences, making it an effective platform for validating aptamer–exosome interactions prior to downstream sensing applications. This makes it a reliable and quantitative way for exosome characterization and biomarker analysis. The objective of this chapter is to validate aptamer-based BLI assays for the detection of breast cancer-derived exosomes using CD63, MUC1, and 5TR1 aptamers. Specifically, this work aims to (i) evaluate the binding response of each aptamer toward exosomes, (ii) assess selectivity using appropriate controls, and (iii) compare marker-dependent binding behavior to determine the suitability of these targets for exosome detection. Establishing reliable and selective aptamer-exosome interactions under controlled conditions is a necessary step toward the development of robust exosome-based diagnostic platforms.

3.2 Materials and Methods

3.2.1 Cell Culture

The MDA-MB-231 (ATCC®, Cat. No. HTB-26TM) cell line was purchased from ATCC, Canada. These cells were cultured in Dulbecco's Modified Eagle Medium (DMEM) growth medium (Thermo Fisher, Cat. No. 11965092) combined with 10% fetal bovine serum (FBS) (Sigma

Aldrich, Cat. No. F1051), 100 µg/mL penicillin, and 100 µg/mL streptomycin. The mixture of DMEM and FBS was diluted in 1:1 and subjected to ultracentrifugation at 100,000 g at 4 ℃ for 20 hours. The MDA-MB-231 cell line was subsequently grown in culture medium within a humidified incubator maintained at 37 °C with 9% CO_2 until reaching 90% surface confluence.

3.2.2 Exosomes Isolation

When the cell growth reach 90% confluency, the cell culture medium was harvested and spun down at 300 g for 5 minutes. Then the supernatant was collected and spun at 2000 g for 30 minutes. After discarding the pellet, the supernatant was transferred to an ultracentrifuge at 16000 g for 1 hour, followed by 3 hours of ultracentrifugation at 100,000 g at 4 ℃ and at the end the pellet was collected and resuspended in phosphate-buffered saline (Thermo Fisher, Cat. No. 10010023) for the final centrifugation step at 100,000 g for 1 hour at 4 ℃. The Collected exosome-PBS solution was stored at -80°C for further analysis.

3.2.3 Dynamic Light Scattering

Dynamic light scattering (DLS) was utilized to assess the size and concentration of MDA-MB-231- derived exosome. The Zetasizer S instrument (Enigma, Malvern, UK) was employed for DLS measurements. The sample was analyzed in a cuvette, and typical 1:10 sample dilutions yielded DLS software (version: 8.02), which facilitated the analysis of MDA-MB-231-derived exosome size and concentration.

3.2.4 Transmission Electron Microscopy

First, the exosomes were fixed in 2% glutaraldehyde for 30 minutes. Then, it was transferred 200-mesh Formvar-coated copper grids (Ted Pella, Cat No. 01800, Redding, California, United States) for 10 minutes. After rinsing twice with filtered HPLC grade water, the grids were negatively stained using Uranyless EM stain (Electron Microscopy Sciences, Cat. No. 22409) for 60 seconds. Excess liquid was removed, and the exosome was visualized using a JOEL JEM 1230 transmission electron microscope operated at 50 kV.

3.2.5 Affinity screening of DNA aptamers binding to breast cancer-derived exosomes by BLI

The measuring of binding affinity of four biotinylated aptamers including, CD63(CACCCCACCTCGCTCCCGTGACACTAATGCTA/3Bio/)[88],MUC1(GCAGTTGATCCTTTGGATACCCTGG/3Bio/)[89],5TR1(GAAGTGAAAATGACAGAACACAACA/3Bio/)[90] and scrambled sequence(ACTTCGCTCCGCACGATCACTTCACCGACACC/3Bio/), purchased from IDT DNA Technology (Iowa, USA), was performed using streptavidin-coated biosensors (SA) (Sartorius, Bohemia, NY). The BLI instrument used was Octet N1 (Sartorius, Bohemia, NY). The BLI workflow was like the previous chapter. Prior to running the experiment on the BLI, the SA sensor tips were subjected to assay buffer (DPBS with 1 mM $CaCl_2$, 0.5 mM $MgCl_2$,0.02% BSA ,0.05% Tween20 and DMEM growth medium pH 7.4) for 10 minutes. Then, the aptamers were prepared in the assay buffer at a concentration of 400 nM, and after heating up at 95°C for 5 minutes, they were cooled on ice for 10 minutes. In this assay, 0.5 mL light-blocking tubes were used with a total volume of 250 µL. The assay was conducted (Figure 12) at room temperature (25 ± 2 °C), and it initiated with a baseline step of 60 seconds in the optimum assay buffer. Then, 400nM of aptamers were loaded

on the SA biosensor tips for 90 s. Three subsequent baselines were performed for 30 seconds each to remove any unbound aptamers prior to the association with 120 seconds, during which a serial dilution of exosomes, including 18.1, 9.05 ,4.52, and 2.26 pM, was loaded and dissociated in the assay buffer. The next step was within 120 seconds.

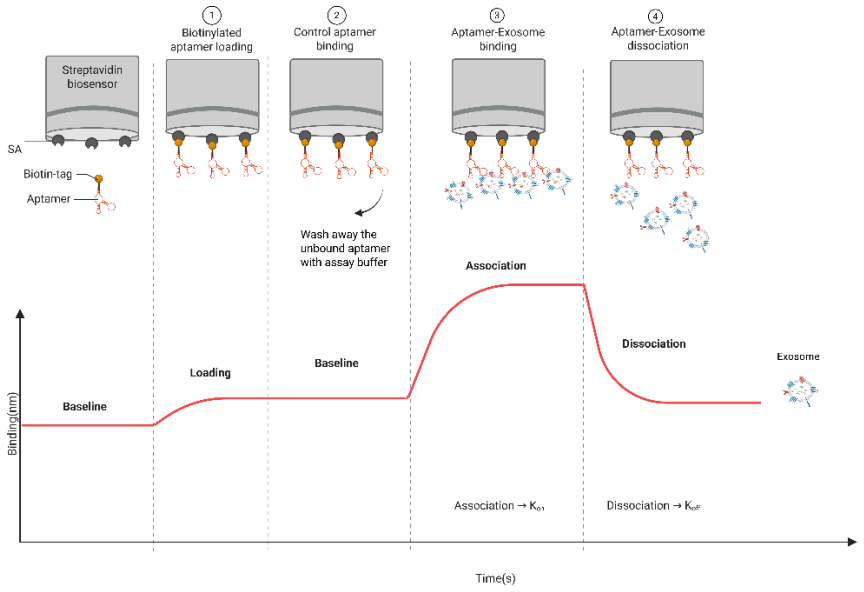

Figure 12.Overview of the Biolayer Interferometry procedure for evaluating aptamer–exosome interactions (created by Bio Render).

3.3 Results

3.3.1 Exosome Isolation

To isolate exosomes, a stepwise differential ultracentrifugation method was used (Figure 13). Upon the MDA-MB-231 cell line reaching approximately 90% cell confluency, the culture medium was harvested from the plate and underwent with low-speed spin at 300×g and 2,000×g to remove cells and cell debris. To withdraw large vesicles, the collected supernatant was spun at high speed at

16,000×g for one hour. Finally, exosomes were pelleted at 100,000×g for several hours, washed, and resuspended in PBS. The exosomes were concentrated to 500 µL using 30 kDa molecular weight cut-off centrifugal filters at 4000 g for 30 minutes for subsequent experiments. Differential ultracentrifugation was selected as a gold standard isolation method to obtain sufficient quantities of exosomes compatible with downstream biophysical analysis. This approach yielded vesicle-enriched fractions suitable for size and morphology characterization prior to binding studies.

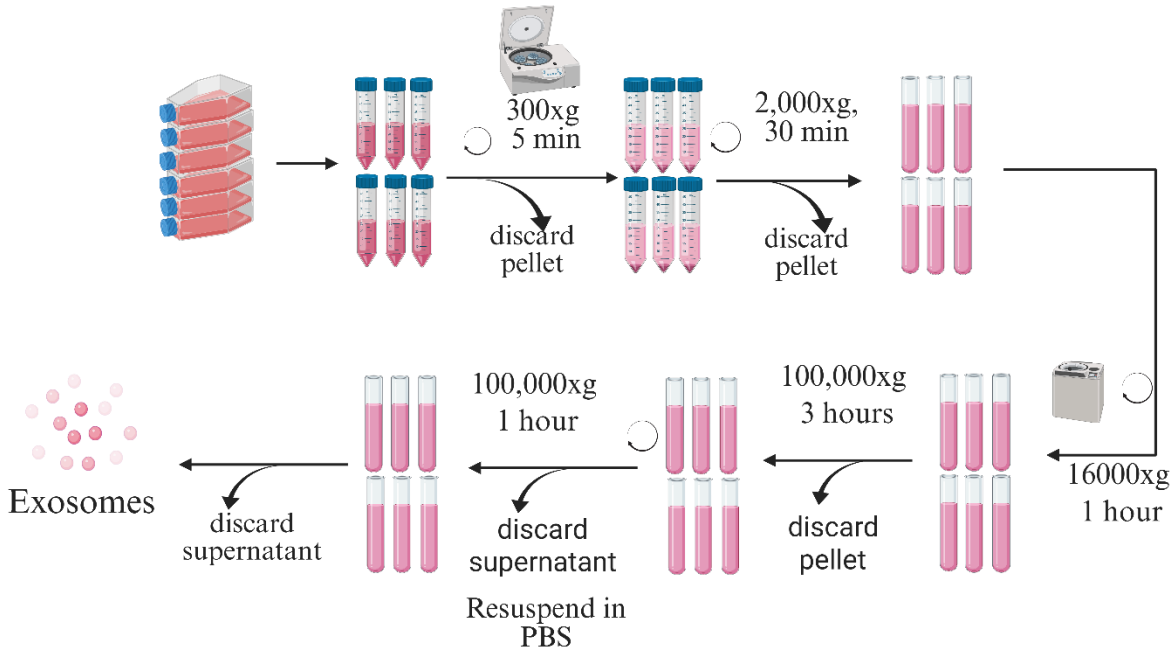

Figure 13.Exosome Isolation Process (created by Bio Render).

3.3.2 Exosome Characterization Based on TEM and DLS Analyses

A combination of techniques, including DLS and TEM, was employed to characterize the isolated exosomes. Dynamic light scattering (DLS) was utilized to assess the size and concentration of exosomes derived from MDA-MB-231. This method revealed that exosomes had the Z-average size of 131 nm and a midpoint of roughly 82 nm with a polydispersity index of 0.36, which indicates that the sample is moderately monodisperse and consistent with exosomes in the 30–150 nm range (Figure 14A). Exosome concentrations were expressed in molar units by estimating particle number from DLS measurements. The particle concentration is converted to molarity using Avogadro's number, assuming each particle behaves as one binding unit. This conversion provides a useful framework for comparing relative binding responses across conditions; however, it should be noted that exosomes are heterogeneous in size and surface composition, and therefore molar concentration represents an approximation rather than a precise molecular quantity. Transmission Electron Microscopy (TEM) is a pivotal technique for the morphological assessment of exosomes. TEM imaging of UranyLess-stained vesicles from isolated fractions was performed to visualize them and examine their membrane structure (Figure 14B). The MDA-MB-231 cell lines exhibited membrane-enclosed vesicles within the exosomal size range of approximately 100 nm.

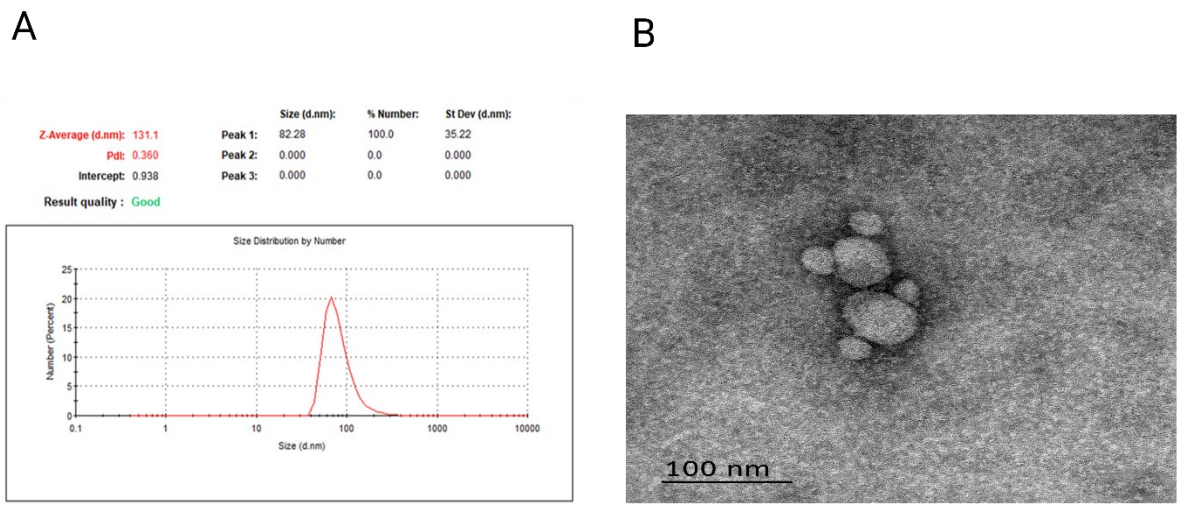

Figure 14.Characterization of Exosomes. (A) Size distribution of isolated exosomes by DLS. (B) TEM images of the enriched MDA-MB-231-derived exosomes.

3.3.3 Characterization of Aptamer-Exosome Interactions through Binding and Kinetic Analyses

The biotinylated surface biomarker aptamers, including CD63, MUC1, and 5TR1, were immobilized on a SA biosensor, and various concentrations of the MDA-MB-231-derived exosomes were prepared in optimum assay buffer to measure binding to aptamers. The binding measurement took place within 15 minutes per sample. The concentration-dependent responses, with higher concentrations producing stronger association signals, for all three aptamers were indicated via binding shifts on the aptamer-based BLI during the interaction with the exosomes (Figure 15). From these shifts, sensorgrams data are created, which allow quantitative extraction of binding parameters, including the equilibrium dissociation constant (table1). As a result, the surface biomarker aptamers could bind to the exosome within a concentration range of 18.1 to 2.26 pM, and the control assay was prepared in the absence of the exosome. Among these three proven

surface biomarker aptamers, CD63 showed the strongest affinity with a K_D of about 1.3 pM, followed by MUC1 at 2.3 pM, and 5TR1 at 2.7 pM. Exosomes present many copies of surface markers, allowing multiple aptamers to bind simultaneously. This multivalency amplifies the signal and changes the binding kinetics compared to single-protein interactions, therefore reported K_D values should be interpreted as apparent affinities. They are useful for comparing relative binding strength between aptamers, but they do not represent true molecular affinity. Kinetic parameters were extracted using the software's default global 1:1 binding model to enable consistent comparison between aptamers under identical experimental conditions. These results should be treated as a proof-of-concept demonstrating that BLI can detect and differentiate exosome-aptamer interactions, rather than as precise quantitative affinity measurements.

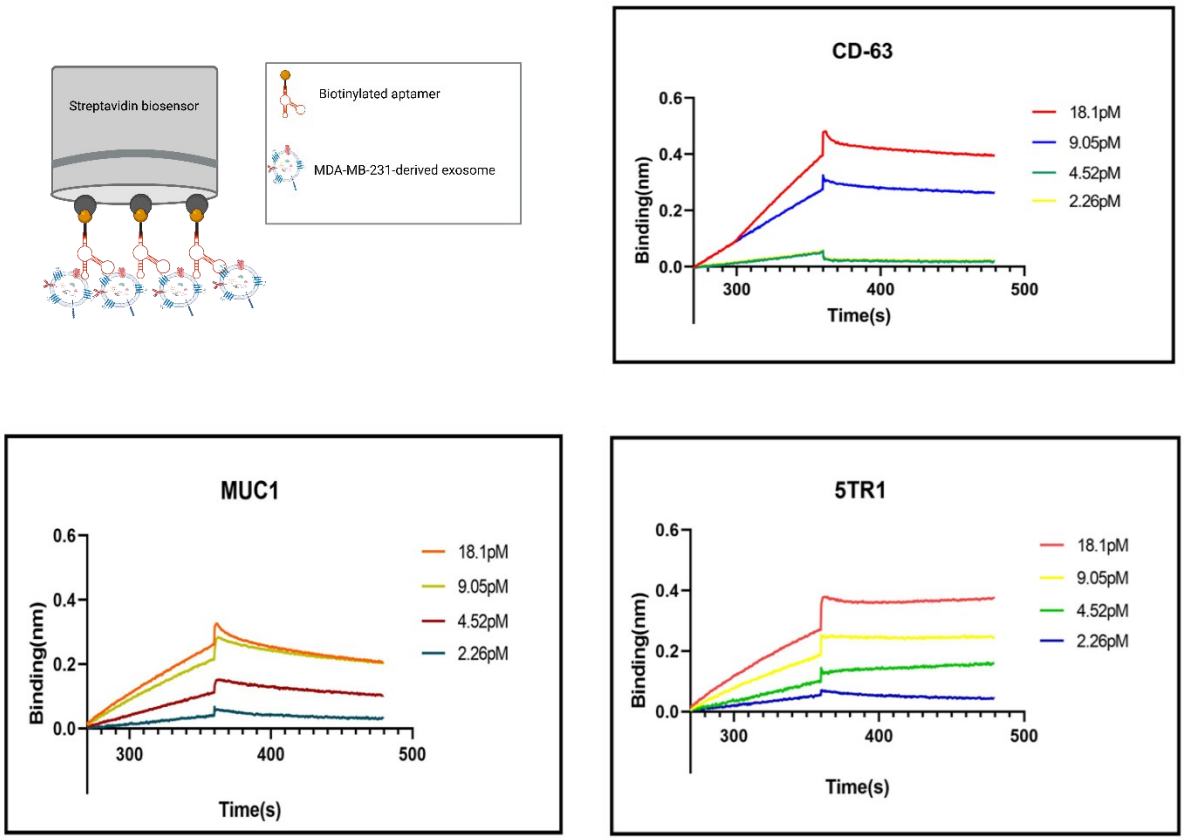

Figure 15. Dynamic measurement of aptamers binding to the MDA-MB-231-derived exosomes.

Table 1. K_Ds of aptamers binding to MDA-MB-231-derived exosomes.

Aptamer	K_D
CD63	1.3 ± 0.7 pM
MUC1	2.3 ± 0.8 pM
5TR1	2.7± 0.7 pM

3.3.4 Evaluation of Quantitative Binding Parameters

To assess the quantitative binding characteristic of the CD63, MUC1, and 5TR1 aptamers, namely Limit of detection (LOD) and Limit of quantification (LOQ), a calibration graph was plotted with variable of BLI response versus exosome concentration (Figure 16). According to this graph, the responses were linear across the working range 2.26-18.1 pM. The CD63 aptamer demonstrated the most sensitive signal amongst three candidate aptamers with the LOD and LOQ of 1.36×10^6 and 4.13×10^6 particles/µl, respectively. MUC1 and 5TR1 also showed good sensitivity, with LODs of $3.\ 41\times10^6$ and 3.90×10^6 particles/µl, in the same order (table2). For all three aptamers, there are strong linear correlations identified by regression equations (Figure 16). In addition, error bars exhibited the standard deviation from three independent replicates (n = 3).

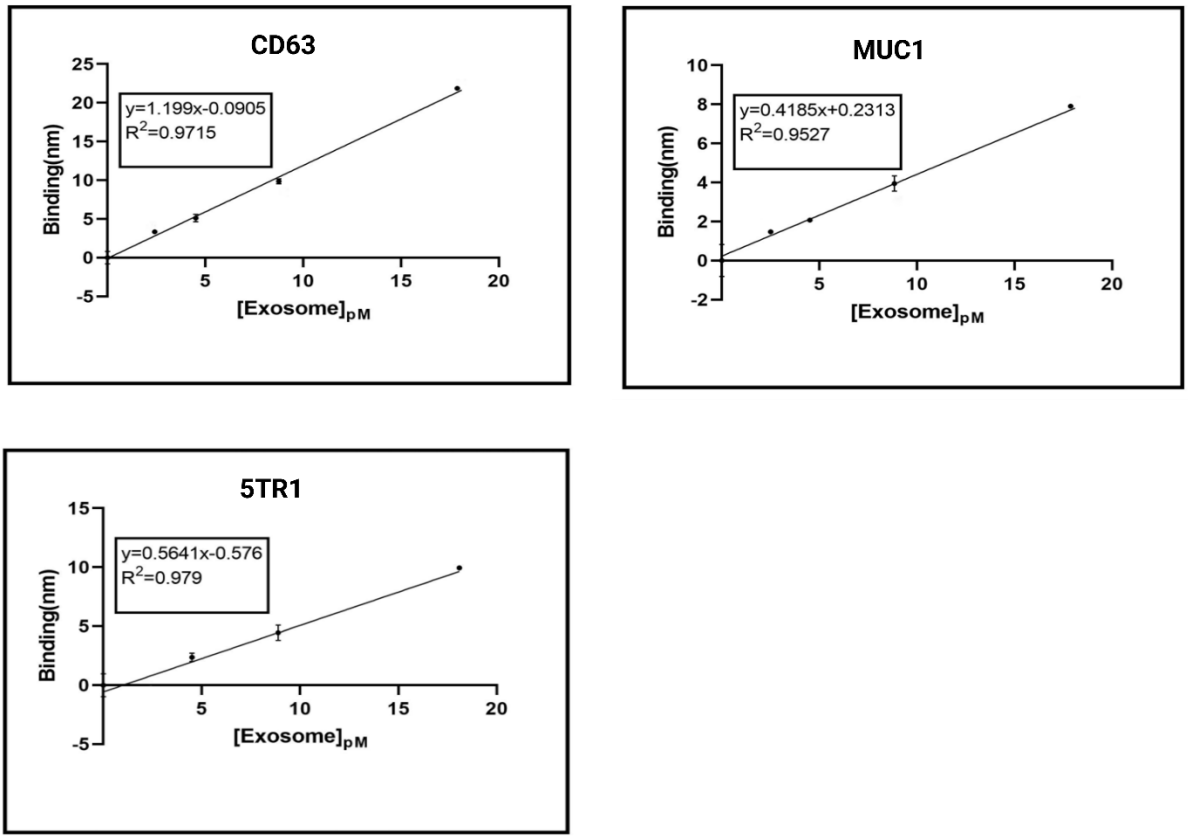

Figure 16.Quantitative calibration plot of CD63, MUC1 and 5TR1.

Table 2.Limit of Detection (LOD) and Limit of Quantification (LOQ) of exosome-binding aptamers.

Aptamer	LOD (particles/µL)	LOQ (particles/µL)
CD63	1.36×10^{6}	4.13×10^{6}
MUC1	3.41×10^{6}	1.03×10^{7}
5TR1	3.90×10^{6}	1.18×10^{7}

3.3.5 Assessment of Aptamers' Specificity Toward Exosomes

A scrambled sequence was introduced as a negative control to confirm the specificity of CD63, MUC1, and 5TR1 aptamers for exosomes. In this assay, exosomes exhibited the strongest binding response to the CD63 aptamer, followed by MUC1 and 5TR1, while the scrambled sequence showed substantially weaker association and faster dissociation (Figure 17). This consistent ranking indicates that binding is not driven solely by non-specific adsorption but rather reflects preferential recognition of specific surface markers.

The lower response observed for the scrambled control supports the conclusion that electrostatic or non-specific interactions contribute only minimally to the overall signal. In contrast, the sustained binding observed for the cancer-associated aptamers suggests marker-dependent multivalent engagement, which is a hallmark of specific exosome recognition.

. The K_D value for the scrambled sequence was by far higher than that of specific aptamers, indicating significantly lower affinity for the scrambled sequence towards the exosomes (Table 3).

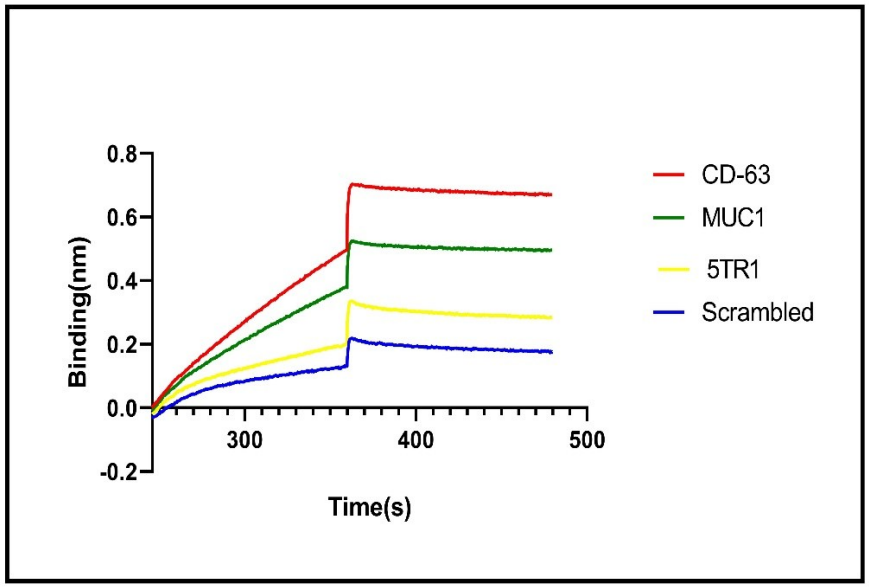

Figure 17.Specific Binding Analysis of aptamers.

Table 3. Comparison of K_Ds for aptamers binding to MDA-MB-231-derived exosome.

Parameter	CD63	MUC1	5TR1	Scrambled
K_D (pM)	1.3 ± 0.7	2.3 ± 0.8	2.7± 0.7	18 ± 12

3.4 Discussion

Exosomes (small extracellular vesicles, ~30–150 nm) ferry proteins, nucleic acids, and lipids that mirror the biology of their parental cells, making them powerful, minimally invasive readouts for tumor status and treatment response[91, 92]. The use of differential ultracentrifugation with sequential low-g and high-g spins to pellet exosomes from MDA-MB-231 media, then confirmed

size/morphology by DLS and TEM. The Z-average 131 nm, midpoint ~82 nm, and PDI of 0.36 indicate a moderately polydisperse nanosized population within the exosome-typical range, and TEM shows membrane-enclosed vesicles ~100 nm. The differential ultracentrifugation strategy employed in this study represents a widely used and well-established approach for exosome isolation rather than a newly developed method. Sequential low-speed centrifugation steps remove cells and debris, followed by high-speed ultracentrifugation to enrich small extracellular vesicles. This approach was selected due to its accessibility, scalability, and compatibility with downstream biophysical characterization. However, it is recognized that differential ultracentrifugation can co-isolate protein aggregates and heterogeneous vesicle populations, necessitating complementary characterization methods such as DLS and TEM to confirm vesicle size and morphology. Alternative isolation techniques, including size-exclusion chromatography, density gradient centrifugation, and immunoaffinity capture, offer improved purity or selectivity but often require longer processing times, specialized materials, or reduced yield. In the context of this work, differential ultracentrifugation provided a practical balance between throughput, yield, and sample compatibility for subsequent BLI-based interaction studies. The biotinylated aptamers immobilized on SA tips and measured binding in DPBS + Ca^{2+}/Mg^{2+} with BSA/Tween-20. Divalent cations promote proper folding of DNA aptamers, while BSA/Tween-20 reduce nonspecific adsorption to the sensor surface, standard practice in BLI and aptamer assays, and heat/snap-cool helps restore the active conformation before runs. These steps collectively improve baseline stability and reduce false-positive association. The concentration-dependent binding of MDA-MB-231-derived exosomes to CD63, MUC1, and 5TR1 aptamers were measured with apparent K_D values in the low-pM range (CD63 1.3 ± 0.7 pM, MUC1 2.3 ± 0.8 pM, 5TR1 2.7 ± 0.7 pM), and a much weaker affinity for the scrambled sequence (18± 12 pM), supporting that

binding is not driven solely by non-specific adsorption, but rather reflects sequence, and preferential structure-dependent recognition of specific surface markers. The association curves did not reach a clear plateau within the experimental timeframe, which is consistent with the multivalent and heterogeneous nature of exosomes rather than incomplete equilibration. Exosomes present multiple copies of surface proteins with variable density, enabling progressive formation of multiple binding contacts that result in a continuously increasing signal. During dissociation, the binding response did not fully return to baseline despite the use of identical buffer conditions, indicating the presence of avidity-driven interactions. Once multiple aptamer-protein contacts are established, dissociation requires simultaneous disruption of several binding events, leading to prolonged surface retention. Under identical assay conditions, the cancer-associated aptamers exhibited stronger association and slower dissociation compared to the scrambled sequence, supporting preferential and marker-dependent binding. Together, these results demonstrate that the observed responses are governed by multivalent recognition rather than non-specific adsorption, validating the use of this assay to assess exosome binding specificity. Although kinetic analysis was performed using a default 1:1 binding model, this model does not fully capture the complexity of exosome-aptamer interactions. Exosomes present multiple copies of surface proteins, enabling multivalent binding events that result in avidity effects. Consequently, the extracted K_D values should be interpreted as apparent affinities rather than true monovalent binding constants. In this context, apparent K_D values remain useful for comparative analysis between aptamers and control sequences under identical experimental conditions. However, they are not sufficient alone to fully describe binding strength or specificity for heterogeneous, multivalent targets such as exosomes. Complementary metrics, including relative response magnitude, association rate trends, and competition assays, may provide additional insight into assay performance. Mechanistically, such

tight apparent affinities can arise from multivalent (multi-point binding). Exosomes carry many copies of the same surface proteins (for example, CD63 and MUC1). When a whole exosome binds to a sensor, several aptamer-protein contacts can form at the same time. This "many-at-once" binding (avidity) makes the measured, apparent K_D look tighter than what you would get for one aptamer binding to one purified protein. In other words, monovalent protein-aptamer pairs often show nanomolar K_D, but intact vesicles can appear much stronger because of multivalency. Song Z. et al selected two DNA aptamers against recombinant CD63 (CD63-1 and CD63-2) with K_D of 38.71 , and 78.43 nM, respectively[93]. The rank order in terms of K_D value (CD63 < MUC1 < 5TR1) also tracks with the known high abundance of CD63 on exosome membranes and the presence of MUC1 on MDA-MB-231-derived exosomes. The quantitative parameters including limit of detection (LOD) and limit of quantification (LOQ) from the calibration curves (2.26–18.1 pM) were obtained for CD63 with LOD 1.36×10^6 and LOQ 4.13×10^6 particles/μL, and MUC1 with LOD 3.41×10^6 particles/μL and LOQ 1.03×10^7particles/μL , and 5TR1 with LOD 3.90×10^6 and LOQ 1.18×10^7particles/μL. This BLI assay is label-free, amplification-free and reports direct, real-time binding, providing kinetic constants alongside quantitative response. Therefore, LODs are expected to be higher than amplified fluorescence/electrochemical formats or antibody sensors, because those platforms leverage enzymatic or nucleic-acid amplification and/or nanoprobe preconcentration[88, 94, 95] . To further evaluate the utility of BLI for exosome detection, future studies could include competition experiments using free antibodies or peptides against CD63, MUC1, or 5TR1 to confirm marker-specific binding. Testing exosome binding in complex biological matrices such as serum or conditioned media without purification would provide insight into biofouling and matrix effects. In addition, comparing responses from exosomes derived from non-cancerous cell lines would help assess false-positive behavior and diagnostic selectivity.

3.5 Conclusion

This chapter demonstrated the feasibility of using an aptamer-based biolayer interferometry platform to detect and characterize breast cancer–derived exosomes through their surface markers. Exosomes isolated from MDA-MB-231 cells were successfully characterized and shown to interact selectively with CD63, MUC1, and 5TR1 aptamers in a concentration-dependent manner. Among the tested aptamers, CD63 produced the strongest binding response, consistent with its high abundance on exosome membranes, while MUC1 and 5TR1 exhibited slightly weaker but still preferential interactions. The use of a scrambled control sequence confirmed that the observed binding was not dominated by non-specific adsorption but instead reflected marker-dependent recognition. The binding behavior observed in this study highlights key features of exosome-surface interactions, including multivalency and avidity, which result in non-ideal association and dissociation profiles and apparent affinities that differ from monovalent protein-ligand systems. Rather than representing a limitation, these characteristics provide important mechanistic insight into how intact vesicles engage biosensor surfaces. While the BLI platform does not achieve the ultra-low detection limits of amplified assays, it offers distinct advantages through label-free, real-time kinetic analysis and straightforward assay design. Overall, this work establishes aptamer-based BLI as a practical and informative tool for evaluating exosome binding behavior and marker selectivity, providing a solid foundation for future studies aimed at improving specificity, assessing performance in complex biological matrices, and advancing exosome-based diagnostic platforms.

Chapter 4

Aptamer-Based Biolayer Interferometry for the Detection of SARS-CoV-2 Pseudoviruses (VLPs)

"The author would like to thank Spencer Uguccioni, a Ph.D. student in Prof. Pezacki's laboratory, for his contribution to the production of SARS-CoV-2 spike pseudovirus (VLPs) used in this study."

4 Abstract

SARS-CoV-2 pseudoviruses (virus-like particles, VLPs) provide a safe and biologically relevant model for studying viral surface recognition while avoiding the biosafety constraints associated with infectious virus handling. Because intact viral particles are nanoscale, multivalent, and structurally complex, their detection presents analytical challenges that are not fully addressed by conventional protein-based assays. In this chapter, an aptamer-based biolayer interferometry (BLI) platform was employed to evaluate the feasibility of detecting SARS-CoV-2 spike pseudoviruses under label-free conditions. Newly selected DNA aptamers targeting the spike protein were investigated to assess binding behavior, selectivity, and analytical performance using intact VLPs rather than isolated recombinant proteins.

Among the three candidate aptamers examined, S1-SP10 exhibited the strongest and most reproducible interaction with SARS-CoV-2 pseudoviruses, with an apparent dissociation constant

of 112 ± 5 nM and a linear response over a concentration range of 50-400 nM. The calculated limits of detection and quantification were 33 nM and 99.4 nM, respectively. Specificity was confirmed through the use of scrambled sequence controls and buffer-only assays, which showed minimal nonspecific binding. Although the extracted affinity values reflect apparent interactions influenced by multivalency and surface presentation, the consistent dose-dependent response and clear differentiation from controls demonstrate that the aptamer-based BLI platform provides a robust and informative approach for probing interactions between aptamers and intact viral particles.

4.1 Introduction

Due to the essential function of the spike protein of SARS-CoV-2, viral entry mechanisms via receptor binding domain (RBD)[77], production of pseudoviruses (VLPs) enables mimicking the process of viral entry under biosafety conditions. In this chapter, a label-free aptasensor based on Biolayer Interferometry (BLI) was employed using newly selected aptamers targeting SARS-CoV-2 pseudoviruses (VLPs), enabling real-time detection through aptamer-analyte interactions. From an analytical perspective, intact viral particles represent challenging sensing targets due to their nanoscale size, multivalent surface architecture, and dependence on conformationally intact surface proteins for recognition. In complex samples, non-specific adsorption, cross-reactivity with host-derived components, and surface fouling can contribute to false-positive signals, while partial epitope masking or structural disruption can lead to false-negative outcomes. These challenges necessitate sensing platforms capable of evaluating selectivity and binding behavior under controlled, label-free conditions. Pseudoviruses provide a practical and biologically relevant model for studying viral surface recognition while avoiding the biosafety constraints associated

with handling infectious SARS-CoV-2. By displaying the spike protein in a membrane context that closely resembles native virions, VLPs preserve key structural and functional features required for binding interactions. As such, pseudoviruses are widely used to evaluate neutralization, receptor binding, and sensing strategies targeting viral entry mechanisms. Aptamer-based recognition elements offer advantages such as chemical stability, reproducible synthesis, and adaptability to surface-based assay formats. When combined with bio-layer interferometry, these properties enable real-time, label-free monitoring of binding interactions while incorporating appropriate reference controls to assess non-specific binding. This makes BLI well suited for validating aptamer interactions with complex, multivalent targets such as virus-like particles. The objective of this chapter is to evaluate the feasibility of using aptamer-based BLI assays for the detection of SARS-CoV-2 pseudoviruses. Specifically, this work aims to (i) characterize the binding response of selected aptamers toward VLPs, (ii) assess selectivity using appropriate controls, and (iii) examine the suitability of this platform for detecting complex viral targets under label-free conditions. Establishing robust aptamer-VLP interactions is a key step toward developing analytical tools for viral detection and surveillance.

4.2 Materials and Methods

4.2.1 Selection of DNA aptamers targeting SARS-CoV-2 pseudoviruses

The aptamer selection method was done by Dr. Suttinee Poolsup (a former Ph.D. student) and it was the same as the previous approach used for selecting aptamers targeting the nucleocapsid of SARS- CoV- 2[96]. In brief, a randomized ssDNA library was heat-folded and subjected to six rounds of selection involving both negative and positive binding steps against the SARS-CoV-2 S1 protein

using Ni-NTA strips. Bound sequences were eluted, concentrated, and amplified through asymmetric emulsion PCR to enrich specific aptamer candidates. Finally, the enriched ssDNA pools were analyzed by next-generation sequencing to identify high-affinity sequences. Three ssDNA aptamers (table 4) were chosen and purchased from IDT DNA Technology (Iowa, USA) for further study.

Table 4.Sequence of selected aptamers.

Aptamer	Aptamer sequence
Biot-S1-Tsp4	/5Biosg/CAC GTA ATG CCT AAC TCT TTT TGT GTT TGC GAT CTT TGC ACA TAG CAT
Biot-S1-Tsp10	/5Biosg/CAC ACT TTC TGC CCG CCT TCT CCC TCC GTT CCC CTC CCC G
Biot-S1-Tsp11	/5Biosg/ATG TCC TCG CAC ACC CAA ACG CAC TCA TCT CCC CAC CCA TGC ATA

4.2.2 SARS-CoV-2 pseudoviruses (VLPs) production

SARS-CoV-2 S pseudovirus (VLPs) production was done by Spencer Uguccioni (a Ph.D. student) and was generated following previously published methods (Figure 18)[97]. In summary, HEK293T cells were seeded at 3 million cells per 10 cm dish. The next day, cells were co-transfected with 2 µg of a pcDNA3.1 plasmid containing codon-optimized cDNA for the SARS-CoV-2 S glycoprotein (or an empty pcDNA3.1) and 4 µg of HIV-NL4.3 ΔEnv Vpr Luciferase Reporter Vector (pNL-4.3.Luc.R-E). Transfections used a ratio of 1.2 µL Lipofectamine 2000 per µg of

plasmid, with plasmids and Lipofectamine 2000 diluted in 12X Opti-MEM, mixed, incubated for 15 minutes, and then added to the plates. After 72 hours, supernatants containing the pseudovirus (VLPs) were collected, centrifuged at 800g for 5 minutes to remove cell debris, and passed through a 0.45 µm filter.

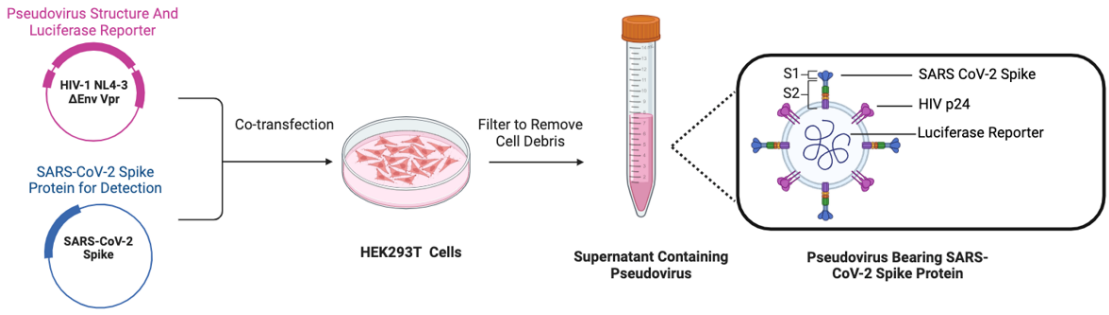

Figure 18. SARS-COV-2 Pseudovirus (VLPs) production (created by Bio render).

4.2.3 Dynamic Light Scattering (DLS)

To determine concentration of the SARS-CoV-2 S pseudovirus (VLPs), Dynamic Light Scattering (DLS) was employed. A Zetasizer S instrument (Enigma, Malvern, UK) was used to perform the measurement. The pseudovirus (VLPs) sample was placed in a cuvette and analyzed following a 1:10 dilution. In order to evaluate concentration of the particles, DLS software (version 8.02) was used for analysis and data acquisition. The concentration of VLPs was reported in molar terms by estimating the number of particles from DLS data. This particle count was then translated into molarity using Avogadro's constant, treating each vesicle as a single binding entity. This representation provides a practical framework for comparing binding responses across concentrations, while acknowledging that VLPs are heterogeneous, multivalent particles rather than discrete molecular species.

4.2.4 Evaluation of DNA Aptamers Affinity Toward SARS-CoV-2 Pseudovirus (VLPs) Using Bio-Layer Interferometry

The aptamer preparation and the BLI setup were similar to the previous projects mentioned in the above chapters. In brief, streptavidin biosensors (SA) and an Octet N1 BLI instrument (Sartorius, Bohemia, NY) were employed to assess the binding affinity. Initially, biotinylated aptamer was prepared in an assay buffer (composed of DPBS with 0.5 mM $MgCl_2$, 1 mM $CaCl_2$, 0.02% BSA, 0.05% Tween20, and DMEM culture media supplemented with 10% FBS at pH 7.4) at a concentration of 400 nM. After heating at 95°C for 5 minutes, it was ice cooled. Prior to BLI aptasensing, the streptavidin (SA) sensor tips were hydrated in the assay buffer for 10-15 minutes. The binding assay took place in 0.5 mL light-blocking tubes at room temperature (25 ± 2 °C), with a total volume of 250 uL. The aptasensing process involved two steps: (i) loading, where the 5′ biotin-modified aptamer was immobilized on the SA sensor surface, and (ii) detection, which included the interaction between the aptamer-loaded sensor and SARS-CoV-2 Pseudovirus (VLPs) (Figure 19). During the binding assay, we established a baseline of 300 seconds in the assay buffer and monitored the association of 600 seconds, loading a serial dilution of SARS-CoV-2 Pseudovirus (VLPs) (50, 100, 200, and 400 nM), and dissociation of 600 seconds on the biosensors. The K_D of the aptamer was calculated using Octet N1 software (version 1.3.0.5) based on a 1:1 global binding model. This orientation ensured that the measured wavelength shift reflected VLP binding to surface-immobilized aptamers rather than nonspecific adsorption of aptamers or viral particles to the sensor surface.

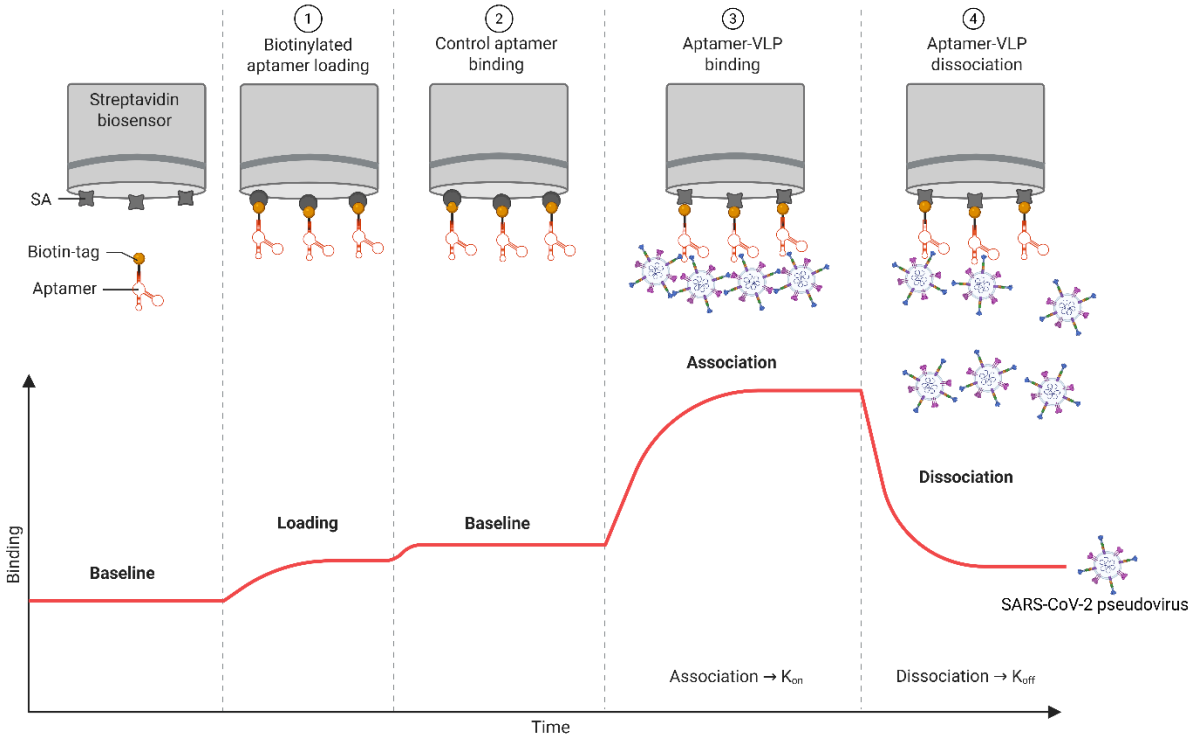

Figure 19.Schematic representation of the Biolayer Interferometry workflow used to assess interactions between aptamer and the SARS-CoV-2 pseudovirus (VLPs) (created with Bio Render).

4.3 Results

4.3.1 Binding evaluation and K_D determination of aptamer to SARS-CoV-2 pseudovirus (VLPs)

The streptavidin biosensor was used to immobilize biotinylated DNA sequences to measure the binding shift to the SARS-CoV-2 pseudovirus (VLPs). Among three selected aptamers including, S1-SP4, S1-SP10, and S1-SP11, S1-SP10 showed stronger binding affinity towards the SARS-CoV-2 pseudovirus (VLPs) (Figure 20A), and as result, it was considered for further evaluations including LOD and LOQ calculations and assessing the binding affinity to dynamic range of concentration of SARS-CoV-2 pseudovirus (VLPs). The binding measurement took place within

roughly 23 minutes per sample. The dose-dependent responses, with higher concentrations producing stronger association signals, for S1-SP10 aptamer was indicated via binding shifts on the aptamer-based BLI during the interaction with SARS-CoV-2 pseudovirus (VLPs) (Figure 20B). From this shift, sensorgram data were created, which allows quantitative extraction of binding parameters, including the equilibrium dissociation constant of 112 ± 5 nM. Therefore, the S1-SP10 aptamer was able to bind to the SARS-CoV-2 pseudovirus (VLPs) within a concentration range of 50 to 400 nM. In addition, the control assay was prepared in three conditions including, in the presence and absence of SARS-CoV-2 pseudovirus (VLPs) and in the absence of the S1-SP10 aptamer. The graph depicted that there was no specific binding of SARS-CoV-2 pseudovirus (VLPs) to the streptavidin biosensor, and additionally, the optimum assay buffer did not exhibit any binding effect on the aptamer (Figure 20C). The K_D value was obtained from kinetic analysis based on the default 1:1 binding model in the Octet N1 software.

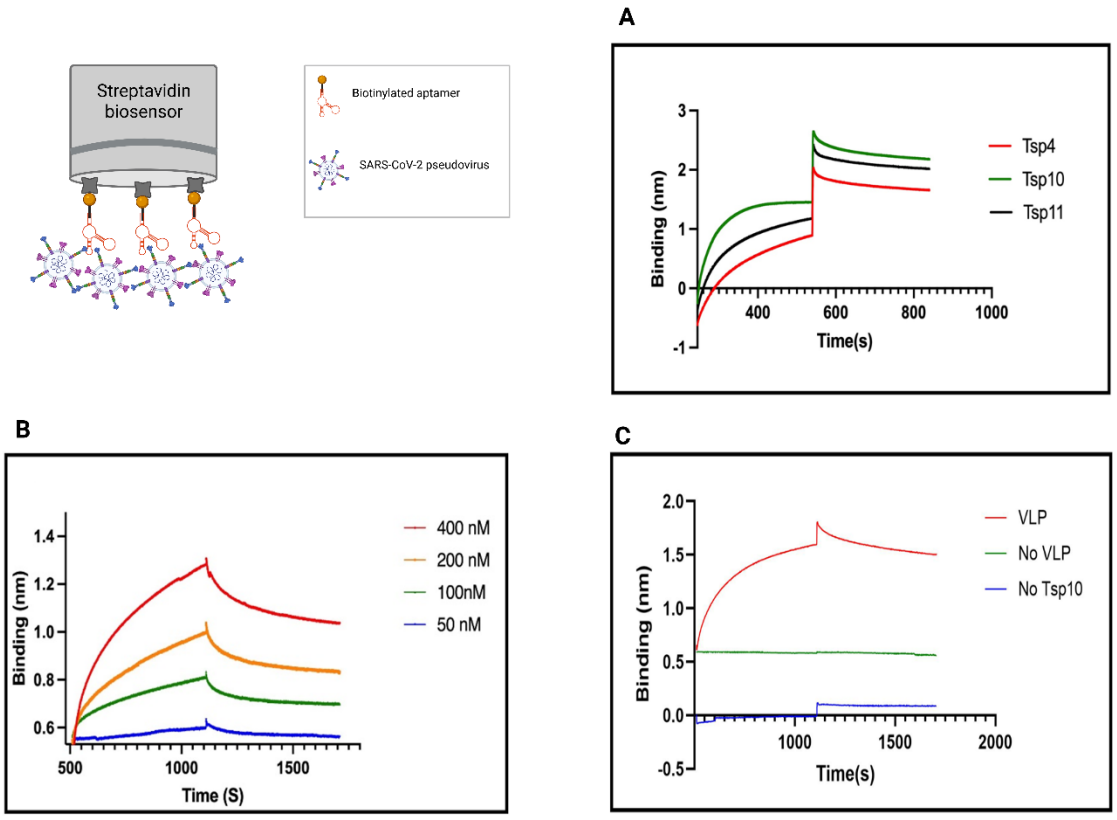

Figure 20.Evaluation of aptamer binding to SARS-CoV-2 pseudovirus (VLPs) by BLI.

4.3.2 Quantitative Analysis of Aptamer-Target Interactions

To calculate the limit of detection (LOD) and limit of quantification (LOQ) for the S1-SP10 aptamer, a calibration curve was plotted with variable of BLI response versus SARS-CoV-2 pseudovirus (VLPs) (Figure 21). The aptasensing assay demonstrated a linear detection range spanning from 50 to 400 nM. The S1-SP10 aptamer demonstrated the high performance with the LOD and LOQ of 33 and 99.4 nM, respectively. The regression equations confirmed a strong linear correlation a R^2 value of 0.96. In addition, error bars exhibited the standard deviation from three independent replicates (n = 3).

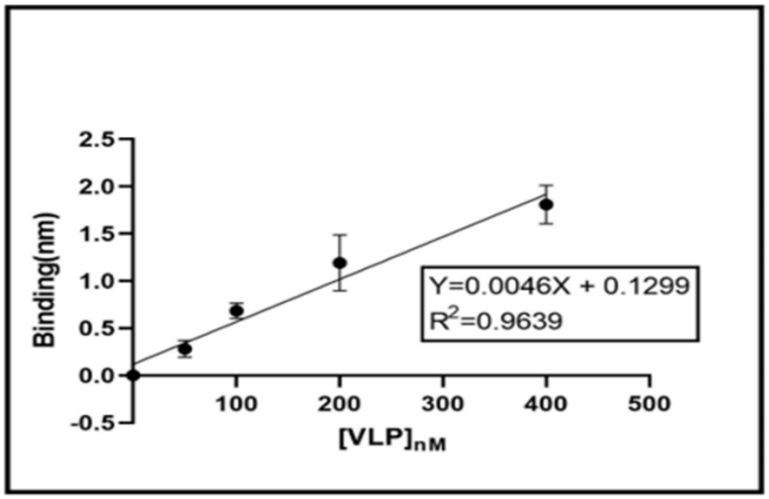

Figure 21.Quantitative relationship between SARS-CoV-2 pseudovirus (VLPs) concentration and binding signal of the S1-SP10 aptamer.

4.3.3 Determination of Aptamer Specificity Against SARS-CoV-2 Pseudovirus (VLPs)

Scrambled sequence was introduced as a negative control to confirm the specificity of S1-SP4, S1-SP10, and S1-SP11 aptamers for SARS-CoV-2 pseudovirus (VLPs). The scrambled sequence was designed to preserve overall length and nucleotide composition comparable to the S1 aptamers while lacking the predicted secondary structure required for target recognition. The same scrambled sequence was used as a general negative control to evaluate whether observed binding responses arose from sequence-specific aptamer folding rather than nonspecific nucleic acid-particle interactions. According to this assay, the observed signal was target-specific by comparing the binding of three selected aptamers vs scrambled sequence. In other words, the target binds strongly to the correct recognition element and not to a random one (Figure 22). The scrambled sequence shows a minimal binding than that of specific aptamers, indicating the scrambled

sequence exhibits a significantly lower affinity for SARS-CoV-2 pseudovirus (VLPs) compared to the other aptamer sequences.

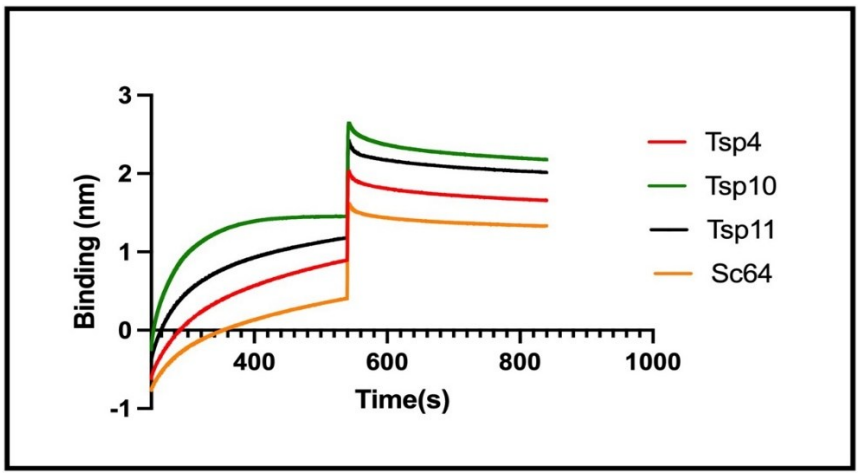

Figure 22.Analysis of Aptamer–SARS-CoV-2 pseudovirus (VLPs) Specific Binding.

Compared to exosome binding experiments, VLPs are multivalent, but they are much more uniform than exosomes. VLPs are engineered particles with a more consistent size and surface composition, so the binding behavior is more reproducible and reaches equilibrium within the experiment time. Exosomes are highly heterogeneous in size and marker density, so the binding is a mixed population effect. Therefore, the VLP sensorgrams exhibited smoother association and dissociation phases, indicating more reproducible interaction kinetics under the tested conditions.

4.4 Discussion

Severe acute respiratory syndrome coronavirus 2 (SARS-CoV-2), the causative agent of COVID-19, remains a major focus of diagnostic and therapeutic research. Its surface spike (S) glycoprotein mediates viral entry through binding to the angiotensin-converting enzyme 2 (ACE2) receptor and

membrane fusion[77]. Because of this essential function, the spike protein is a key target for detection platforms. To mimic the viral entry process safely, SARS-CoV-2 pseudoviruses (VLPs) are used, these are replication-incompetent particles displaying the spike protein on their surface, allowing molecular interaction studies under biosafety conditions[98]. Although both exosomes and SARS-CoV-2 pseudoviruses are multivalent nanoscale particles, differences in surface organization likely contribute to the improved association behavior observed for VLPs. VLPs present the spike protein in a relatively uniform and repetitive architecture, whereas exosomes exhibit highly heterogeneous and dynamic protein distributions. As a result, VLP-aptamer interactions may involve lower effective heterogeneity and more consistent multivalent engagement, producing smoother sensorgram profiles[99]. Therefore, developing sensitive and selective biosensing methods for detecting SARS-CoV-2 pseudoviruses (VLPs) contributes both to diagnostic advancement and to understanding virus-ligand interactions in a safe experimental setting. In this study, a label-free Biolayer Interferometry (BLI) platform was employed to evaluate three newly selected DNA aptamers (S1-SP4, S1-SP10, and S1-SP11) targeting SARS-CoV-2 pseudoviruses (VLPs). BLI offers real-time kinetic measurement without labeling or complex surface chemistry, providing quantitative parameters such as the equilibrium dissociation constant (K_D), limit of detection (LOD), and limit of quantification (LOQ). Among the candidates, the S1-SP10 aptamer exhibited the strongest binding affinity with a K_D of 112 ± 5 nM**,** outperforming the other two sequences. Despite the improved kinetic profiles, SARS-CoV-2 pseudoviruses remain multivalent targets due to the presence of multiple spike trimers on each particle. Consequently, the K_D values extracted using a 1:1 binding model should be interpreted as apparent affinities that describe the overall interaction behavior rather than true monovalent binding constants. This apparent affinity remains useful for comparative evaluation of aptamer performance under identical experimental

conditions[100]. The dose-dependent sensorgram responses confirmed the specific and reversible binding behavior typical of aptamer-protein interactions. When working with intact VLPs, incomplete return to baseline during dissociation is often expected because a single particle can form multiple simultaneous contacts with the aptamer-coated surface; once several interactions are engaged, release requires breaking many bonds (not just one), so the complex dissociates slowly and may not fully wash off within the measurement window. This is a classic avidity-dominated signature. In this context, the persistent signal does not indicate poor data quality; rather, it reflects the biologically realistic, multivalent nature of VLP-receptor binding, but it does mean that the reported $K_D$should be interpreted as an apparent affinity influenced by avidity and surface presentation rather than a strict 1:1 equilibrium constant. The absence of significant signal in control assays (aptamer-free, virus-free, and buffer-only conditions) verified the specificity of the observed responses. The measured K_D of 112 nM demonstrates moderate-to-high affinity for the spike protein, consistent with other reported aptamer-based SARS-CoV-2 sensors. For instance, Wu et al, selected an aptamer against the SARS-CoV-2 S1 protein on an automatic integrated microfluidic SELEX platform and reported K_D values of 63 nM [101]. A DNA aptamer was selected against the Spike RBD with K_D of 5.8 nM (CoV2-RBD-1C) and 19.9 nM (CoV2-RBD-4C), measured via bead-based binding/flow-cytometry analysis by a Song et al[102]. Aptamer SP6 targeting the full trimeric Spike ectodomain with K_D of 13.9 nM determined by surface plasmon resonance (SPR) was reported by Schmitz et al[103]. Most published SARS-CoV-2 aptamer studies evaluated aptamer binding to purified recombinant RBD or S1 proteins immobilized on chips or beads. These proteins are isolated, with their binding sites fully exposed. In contrast, this assay used SARS-CoV-2 pseudoviruses (VLPs), nanoscale particles presenting the trimeric spike in a native membrane context. On these surfaces, many RBD sites are partially shielded or

conformationally restricted by the viral envelope, glycosylation, or local crowding, which reduces effective accessibility. This difference alone often produces apparent K_D values that are 5 to 20-fold higher than those measured for soluble proteins. Therefore, the obtained K_D aligns well with these benchmarks, confirming that the S1-SP10 aptamer provides a strong and specific interaction suitable for analytical purposes. The linear quantitative relationship between BLI signal and SARS-CoV-2 pseudovirus (VLPs) concentration (R^2 = 0.96) across the 50–400 nM range highlights the reliability of the S1-SP10 aptasensor. The determined LOD (33 nM) and LOQ (99.4 nM) indicate high analytical sensitivity for a label-free format. Similar Label-free optical aptasensors for SARS-CoV-2 components have achieved LODs between 10 and 100 nM. For instance, Cennamo et al. reported LOD of 37 nM for Spike RBD using an aptamer-functionalized plasmonic (LSPR) fiber[104], placing our values within realistic expectations for label-free optics. The lack of nonspecific adsorption from the assay buffer also demonstrates the optimized composition of the BLI running solution (DPBS + Mg^{2+}/Ca^{2+} + BSA + Tween-20 + DMEM-FBS), which minimizes background noise and preserves aptamer folding stability. The scrambled sequence control addresses whether the observed binding arises from sequence- and structure-dependent aptamer recognition rather than nonspecific interactions between nucleic acids and VLPs. The reduced response observed for the scrambled sequence supports the conclusion that VLPs selectively interact with the folded S1 aptamer, rather than demonstrating selective binding of the scrambled sequence itself. This distinction is critical when assessing assay specificity for biomarker detection. From a biomarker detection perspective, the relevant specificity criterion is whether the sensing platform can reliably distinguish SARS-CoV-2 pseudoviruses from background signals and nonspecific nucleic acid interactions. The combined use of sequence-specific aptamers, scrambled controls, and optimized buffer conditions supports preferential

recognition of the viral spike protein in a particle-based context, while acknowledging that further validation in complex biological matrices would be required for diagnostic translation.

4.5 Conclusion

This chapter demonstrated the application of an aptamer-based biolayer interferometry platform for the detection and characterization of SARS-CoV-2 spike pseudoviruses. Using intact VLPs as analytically relevant targets, the study showed that selected DNA aptamers can recognize viral particles in a native membrane context, with S1-SP10 exhibiting the strongest binding response among the tested sequences. The observed concentration-dependent sensorgrams, combined with minimal background signal in control experiments, confirm that the measured interactions arise primarily from sequence-dependent aptamer recognition rather than nonspecific adsorption. The binding behavior observed for SARS-CoV-2 pseudoviruses reflects the inherently multivalent nature of viral particles, leading to apparent affinities and dissociation profiles that differ from those of monovalent protein systems. Rather than undermining the quality of the results, these features provide meaningful insight into how intact viral particles engage surface-immobilized recognition elements. The reported kinetic and analytical parameters should therefore be interpreted as apparent values that describe overall particle-surface interactions under defined conditions. Overall, this work establishes aptamer-based BLI as a practical, label-free platform for studying viral particle binding behavior and evaluating aptamer performance, offering a solid foundation for future studies aimed at improving sensitivity, testing complex biological matrices, and advancing viral sensing strategies.

Chapter 5

5 Overall Conclusion

This thesis set out to evaluate aptamer-based biolayer interferometry (BLI) as a unified analytical platform for studying biomolecular interactions across increasing levels of biological complexity, ranging from purified protein targets to intact extracellular vesicles and viral particles. Across all three experimental systems, Ki-67 protein, cancer-derived exosomes, and SARS-CoV-2 spike pseudoviruses, the results consistently demonstrated that aptamer-BLI provides a flexible, label-free, and mechanistically informative approach for probing binding behavior under controlled conditions. Rather than focusing solely on detection sensitivity, this work emphasized understanding how molecular recognition unfolds in real time, particularly in systems where non-ideal binding behavior is intrinsic to the target itself. The Ki-67 study established a foundation for this approach by demonstrating that aptamer-BLI can quantitatively resolve binding interactions even for proteins with strong electrostatic character. The observed nanomolar affinity of the Ki-67 aptamer, together with its preferential binding over a scrambled control, showed that sequence and structural features of the aptamer contribute meaningfully to interaction strength despite unavoidable background electrostatic interactions. Importantly, this chapter highlighted that selectivity should not be interpreted as an absence of non-specific binding, but rather as a measurable preference that can be evaluated through appropriate controls and comparative analysis. This perspective provided a realistic and rigorous framework for interpreting binding data

for highly charged proteins and underscored the value of BLI in separating baseline interactions from sequence-dependent recognition. Building on this protein-level analysis, the exosome chapter extended the platform to intact nanoscale vesicles, where multivalency, surface heterogeneity, and avidity effects play a dominant role. The preferential binding observed for CD63, MUC1, and 5TR1 aptamers, together with weaker responses from scrambled controls, demonstrated that aptamer-BLI can discriminate between marker-dependent and non-specific interactions in complex vesicle systems. The absence of ideal association plateaus and incomplete dissociation profiles were interpreted not as experimental limitations, but as signatures of biologically relevant multivalent engagement. By embracing these features rather than attempting to force monovalent kinetic models, this work showed that BLI can provide meaningful insight into how exosomes interact with biosensor surfaces and how different surface markers contribute to binding behavior. A similar interpretation emerged from the SARS-CoV-2 pseudovirus study, where intact viral particles were used as analytically relevant targets. The ability of selected DNA aptamers, particularly S1-SP10, to recognize spike pseudoviruses in their native membrane context further demonstrated the adaptability of the aptamer-BLI platform. As with exosomes, the observed avidity-driven binding behavior resulted in apparent affinities and dissociation kinetics that differ from those of isolated protein systems. Rather than diminishing the quality of the data, these results reinforced the importance of interpreting kinetic parameters as system-level descriptors of particle-surface interactions. The clear differentiation between specific aptamer responses and minimal background binding from controls confirmed that the platform remains robust even in highly multivalent viral systems. Taken together, these three case studies illustrate that aptamer-based BLI is not limited to a single class of targets but can be applied across a spectrum of biological entities while maintaining interpretive consistency. A central theme emerging from this work is

that biological complexity, whether arising from electrostatic charge, surface heterogeneity, or multivalency, should be explicitly considered during data interpretation rather than treated as a confounding factor. By using appropriate controls, blocking strategies, and comparative analysis, the platform enables these complexities to be quantified and contextualized, leading to a more realistic understanding of molecular recognition. While the BLI platform does not achieve the ultra-low detection limits of signal-amplified assays, its strength lies in its simplicity, reproducibility, and ability to generate real-time kinetic information without labeling or extensive sample processing. The results presented in this thesis demonstrate that aptamer-BLI is particularly well suited for early-stage evaluation of binding behavior, selectivity, and surface interaction mechanisms, key parameters that underpin the rational design of biosensing systems. Future work may focus on improving sensitivity through surface engineering, exploring performance in complex biological matrices, and integrating multiplexed aptamer arrays to enhance selectivity for clinical applications. In conclusion, this thesis establishes aptamer-based biolayer interferometry as a versatile and informative analytical platform for studying molecular interactions across different biological scales. By prioritizing mechanistic understanding over purely analytical metrics, this work provides a framework for interpreting binding behavior in complex systems and lays the groundwork for the continued development of aptamer-based biosensing technologies targeting proteins, extracellular vesicles, and viral particles.

5.1 Limitation

While this study showed strong and consistent results, some technical challenges were faced during the experiments. The BLI method, although simple and label-free, can be affected by repeated sensor regeneration, which sometimes reduces the sensor's performance and causes small variations between runs. Exosome preparation was also a major limitation since exosomes are

delicate and can easily degrade. Collecting a large amount of pure exosomes required several days of isolation, which made it difficult to perform multiple replicates for each experiment. In addition, producing SARS-CoV-2 pseudoviruses was time-consuming and required careful handling to maintain particle stability and biosafety. These factors sometimes limited the number of tests that could be done and made the overall workflow slower.

5.2 Future directions

The results of this thesis create a strong base for improving aptamer-based Biolayer Interferometry (BLI) biosensors used in cancer and virus detection. Each project proved that label-free BLI systems can measure molecular interactions accurately and reliably. However, there is still room to make these systems more biologically relevant, precise, and ready for real-world applications. The following points describe the next practical steps for future research.

For the Ki-67 aptamer project, future experiments can go beyond purified protein tests and focus on more realistic biological environments. The next step would be to test the aptamer directly in cancer cell lines that naturally express different levels of Ki-67. Techniques such as fluorescence microscopy or flow cytometry could be used to see if the aptamer can recognize Ki-67 inside cells and to compare its performance with commercial antibodies. This would confirm whether the aptamer stays specific and effective under real biological conditions. It would also be helpful to test the aptamer against other similar nuclear or cell cycle proteins to ensure it only binds to Ki-67. Shortening or slightly modifying the aptamer sequence could also make it more stable and efficient while keeping its binding ability.

In the exosome detection project, this work showed that BLI can be used to study exosomes from MDA-MB-231 breast cancer cells using CD63, MUC1, and 5TR1 aptamers. To bring this system

closer to real biomedical use, more validation is needed with other methods like flow cytometry, nanoparticle tracking analysis (NTA), and mass spectrometry. These methods can confirm that the isolated exosomes are pure and correctly identified, which supports the accuracy of the aptamer results. Future work could also compare cancerous exosomes with those from normal cell lines, such as MCF10A, to check if the sensor can truly tell the difference between healthy and cancer-derived vesicles. Expanding these tests to real patient samples like plasma or serum would also show how well the sensor performs in more complex biological fluids. To improve isolation precision, methods such as size-exclusion chromatography (SEC) could be added to the workflow. Combining BLI with other sensitive detection techniques like surface-enhanced Raman spectroscopy (SERS) or electrochemical impedance spectroscopy (EIS) could also provide deeper information about both the binding strength and the molecular structure of the exosome-aptamer interaction.

The study of SARS-CoV-2 pseudovirus project confirmed that BLI combined with specific DNA aptamers can successfully detect virus-like particles. Future work should test these sensors in more complex biological samples such as saliva, nasal swabs, or blood serum. These samples are closer to real diagnostic situations and can reveal how well the assay performs when faced with challenges like background interference or nonspecific binding.

Finally, collaboration with clinical research groups and hospitals will be an important step toward turning these findings into real diagnostic tools. Testing the developed sensors on patient samples including tumor tissues, exosomes from blood, or viral particles would prove their reliability and value for clinical use. With further optimization to increase selectivity, stability, and sensitivity, the aptamer-based BLI systems developed in this thesis could form the foundation of a new

generation of fast, label-free, and highly specific diagnostic technologies for cancer, viral infections, and personalized medicine.

References

1. Tuerk, C.; Gold, L., Systematic evolution of ligands by exponential enrichment: RNA ligands to bacteriophage T4 DNA polymerase. *science* **1990,** *249* (4968), 505-510.
2. Ellington, A. D.; Szostak, J. W., In vitro selection of RNA molecules that bind specific ligands. *nature* **1990,** *346* (6287), 818-822.
3. Cho, E. J.; Lee, J.-W.; Ellington, A. D., Applications of aptamers as sensors. *Annual review of analytical chemistry* **2009,** *2* (1), 241-264.
4. Zhou, J.; Rossi, J., Aptamers as targeted therapeutics: current potential and challenges. *Nature reviews Drug discovery* **2017,** *16* (3), 181-202.
5. Song, S.; Wang, L.; Li, J.; Fan, C.; Zhao, J., Aptamer-based biosensors. *TrAC Trends in Analytical Chemistry* **2008,** *27* (2), 108-117.
6. Keefe, A. D.; Pai, S.; Ellington, A., Aptamers as therapeutics. *Nature reviews Drug discovery* **2010,** *9* (7), 537-550.
7. Nimjee, S. M.; Rusconi, C. P.; Sullenger, B. A., Aptamers: an emerging class of therapeutics. *Annu. Rev. Med.* **2005,** *56* (1), 555-583.
8. Russo, M. J.; Han, M.; Desroches, P. E.; Manasa, C. S.; Dennaoui, J.; Quigley, A. F.; Kapsa, R. M.; Moulton, S. E.; Guijt, R. M.; Greene, G. W., Antifouling strategies for electrochemical biosensing: mechanisms and performance toward point of care based diagnostic applications. *ACS sensors* **2021,** *6* (4), 1482-1507.
9. Vasilescu, A.; Gáspár, S.; Gheorghiu, M.; Polonschii, C.; Banciu, R. M.; David, S.; Gheorghiu, E.; Marty, J.-L., Promising Solutions to Address the Non-Specific Adsorption in Biosensors Based on Coupled Electrochemical-Surface Plasmon Resonance Detection. *Chemosensors* **2025,** *13* (3), 92.
10. Elskens, J. P.; Elskens, J. M.; Madder, A., Chemical modification of aptamers for increased binding affinity in diagnostic applications: Current status and future prospects. *International Journal of Molecular Sciences* **2020,** *21* (12), 4522.
11. Yaghoobi, E.; Shojaee, S.; Ramezani, M.; Alibolandi, M.; Charbgoo, F.; Nameghi, M. A.; Khatami, F.; Ashjaei, M. S.; Abnous, K.; Taghdisi, S. M., A novel targeted co-delivery system for transfer of epirubicin and antimiR-10b into cancer cells through a linear DNA nanostructure consisting of FOXM1 and AS1411 aptamers. *Journal of Drug Delivery Science and Technology* **2021,** *63*, 102521.
12. Gordon, C. K.; Eisenstein, M.; Soh, H. T., Direct selection strategy for isolating aptamers with pH-sensitive binding activity. *ACS sensors* **2018,** *3* (12), 2574-2580.
13. Darmostuk, M.; Rimpelova, S.; Gbelcova, H.; Ruml, T., Current approaches in SELEX: An update to aptamer selection technology. *Biotechnology advances* **2015,** *33* (6), 1141-1161.
14. Zhuo, Z.; Yu, Y.; Wang, M.; Li, J.; Zhang, Z.; Liu, J.; Wu, X.; Lu, A.; Zhang, G.; Zhang, B., Recent advances in SELEX technology and aptamer applications in biomedicine. *International journal of molecular sciences* **2017,** *18* (10), 2142.
15. Kohlberger, M.; Gadermaier, G., SELEX: Critical factors and optimization strategies for successful aptamer selection. *Biotechnology and applied biochemistry* **2022,** *69* (5), 1771-1792.

16. Zhao, Y.; Yavari, K.; Liu, J., Critical evaluation of aptamer binding for biosensor designs. *TrAC Trends in Analytical Chemistry* **2022,** *146*, 116480.
17. Bashir, A.; Yang, Q.; Wang, J.; Hoyer, S.; Chou, W.; McLean, C.; Davis, G.; Gong, Q.; Armstrong, Z.; Jang, J., Machine learning guided aptamer refinement and discovery. *Nature Communications* **2021,** *12* (1), 2366.
18. Li, X.; Liu, S.; Huang, X.; Yao, C.; Chen, J.; Gao, L.; Zhou, C.; Wu, Y.; Liu, J.; Li, M., Aptamers-based wearable electrochemical sensors for continuous monitoring of biomarkers in vivo. *Microsystems & Nanoengineering* **2025,** *11* (1), 241.
19. Catuogno, S.; Esposito, C. L., Aptamer cell-based selection: overview and advances. *Biomedicines* **2017,** *5* (3), 49.
20. Domsicova, M.; Korcekova, J.; Poturnayova, A.; Breier, A., New insights into aptamers: An alternative to antibodies in the detection of molecular biomarkers. *International Journal of Molecular Sciences* **2024,** *25* (13), 6833.
21. Fallah, A.; Fooladi, A. A. I.; Havaei, S. A.; Mahboobi, M.; Sedighian, H., Recent advances in aptamer discovery, modification and improving performance. *Biochemistry and Biophysics Reports* **2024,** *40*, 101852.
22. Jabbari, A.; Sameiyan, E.; Yaghoobi, E.; Ramezani, M.; Alibolandi, M.; Abnous, K.; Taghdisi, S. M., Aptamer-based targeted delivery systems for cancer treatment using DNA origami and DNA nanostructures. *International Journal of Pharmaceutics* **2023,** *646*, 123448.
23. Khoshnood, A.; Farhadian, N.; Abnous, K.; Matin, M. M.; Ziaee, N.; Yaghoobi, E., N doped-carbon quantum dots with ultra-high quantum yield photoluminescent property conjugated with folic acid for targeted drug delivery and bioimaging applications. *Journal of Photochemistry and Photobiology A: Chemistry* **2023,** *444*, 114972.
24. Esmaelpourfarkhani, M.; Abnous, K.; Taghdisi, S. M.; Chamsaz, M., A novel turn-off fluorescent aptasensor for ampicillin detection based on perylenetetracarboxylic acid diimide and gold nanoparticles. *Biosensors and Bioelectronics* **2020,** *164*, 112329.
25. Yaghoobi, E.; Zavvar, T.; Ramezani, M.; Alibolandi, M.; Rahimzadeh Oskuei, S.; Zahiri, M.; Alinezhad Nameghi, M.; Abnous, K.; Taghdisi, S. M., A multi-storey DNA nanostructure containing doxorubicin and AS1411 aptamer for targeting breast cancer cells. *Journal of Drug Targeting* **2022,** *30* (10), 1106-1112.
26. Feng, C.; Dai, S.; Wang, L., Optical aptasensors for quantitative detection of small biomolecules: A review. *Biosensors and Bioelectronics* **2014,** *59*, 64-74.
27. Chang, A. L.; McKeague, M.; Liang, J. C.; Smolke, C. D., Kinetic and equilibrium binding characterization of aptamers to small molecules using a label-free, sensitive, and scalable platform. *Analytical chemistry* **2014,** *86* (7), 3273-3278.
28. Guérin, M.; Vandevenne, M.; Matagne, A.; Aucher, W.; Verdon, J.; Paoli, E.; Ducrotoy, J.; Octave, S.; Avalle, B.; Maffucci, I., Selection and characterization of DNA aptamers targeting the surface Borrelia protein CspZ with high-throughput cross-over SELEX. *Communications Biology* **2025,** *8* (1), 632.
29. Wei, T.; Liu, Q.; Li, J.; Song, S.; Zhang, L., Functional Aptamers In Vitro Evolution for Protein–Protein Interaction Blockage. *Analytical Chemistry* **2025,** *97* (8), 4341-4349.
30. Concepcion, J.; Witte, K.; Wartchow, C.; Choo, S.; Yao, D.; Persson, H.; Wei, J.; Li, P.; Heidecker, B.; Ma, W., Label-free detection of biomolecular interactions using BioLayer interferometry for kinetic characterization. *Combinatorial chemistry & high throughput screening* **2009,** *12* (8), 791-800.

31. Jug, A.; Bratkovič, T.; Ilaš, J., Biolayer interferometry and its applications in drug discovery and development. *TrAC Trends in Analytical Chemistry* **2024,** *176*, 117741.
32. Masson, J.-F., Consideration of sample matrix effects and "biological" noise in optimizing the limit of detection of biosensors. ACS Publications: 2020; Vol. 5, pp 3290-3292.
33. Wang, W.; He, Y.; He, S.; Deng, L.; Wang, H.; Cao, Z.; Feng, Z.; Xiong, B.; Yin, Y., A brief review of aptamer-based biosensors in recent years. *Biosensors* **2025,** *15* (2), 120.
34. Ullah, S. F.; Moreira, G.; Datta, S. P. A.; McLamore, E.; Vanegas, D., An experimental framework for developing point-of-need biosensors: connecting bio-layer interferometry and electrochemical impedance spectroscopy. *Biosensors* **2022,** *12* (11), 938.
35. Abdiche, Y.; Malashock, D.; Pinkerton, A.; Pons, J., Determining kinetics and affinities of protein interactions using a parallel real-time label-free biosensor, the Octet. *Analytical biochemistry* **2008,** *377* (2), 209-217.
36. Müller-Esparza, H.; Osorio-Valeriano, M.; Steube, N.; Thanbichler, M.; Randau, L., Bio-layer interferometry analysis of the target binding activity of CRISPR-Cas effector complexes. *Frontiers in molecular biosciences* **2020,** *7*, 98.
37. Kamat, V.; Rafique, A., Designing binding kinetic assay on the bio-layer interferometry (BLI) biosensor to characterize antibody-antigen interactions. *Analytical biochemistry* **2017,** *536*, 16-31.
38. Petersen, R. L., Strategies using bio-layer interferometry biosensor technology for vaccine research and development. *Biosensors* **2017,** *7* (4), 49.
39. Dubrow, A.; Zuniga, B.; Topo, E.; Cho, J.-H., Suppressing nonspecific binding in biolayer interferometry experiments for weak ligand–analyte interactions. *ACS omega* **2022,** *7* (11), 9206-9211.
40. Schonk, D.; Kuijpers, H.; Van Drunen, E.; Van Dalen, C.; Geurts van Kessel, A.; Verheijen, R.; Ramaekers, F., Assignment of the gene (s) involved in the expression of the proliferation-related Ki-67 antigen to human chromosome 10. *Human genetics* **1989,** *83* (3), 297-299.
41. Gerdes, J.; Schwab, U.; Lemke, H.; Stein, H., Production of a mouse monoclonal antibody reactive with a human nuclear antigen associated with cell proliferation. *International journal of cancer* **1983,** *31* (1), 13-20.
42. Takagi, M.; Sueishi, M.; Saiwaki, T.; Kametaka, A.; Yoneda, Y., A novel nucleolar protein, NIFK, interacts with the forkhead associated domain of Ki-67 antigen in mitosis. *Journal of Biological Chemistry* **2001,** *276* (27), 25386-25391.
43. Sueishi, M.; Takagi, M.; Yoneda, Y., The forkhead-associated domain of Ki-67 antigen interacts with the novel kinesin-like protein Hklp2. *Journal of biological chemistry* **2000,** *275* (37), 28888-28892.
44. Booth, D. G.; Takagi, M.; Sanchez-Pulido, L.; Petfalski, E.; Vargiu, G.; Samejima, K.; Imamoto, N.; Ponting, C. P.; Tollervey, D.; Earnshaw, W. C., Ki-67 is a PP1-interacting protein that organises the mitotic chromosome periphery. *Elife* **2014,** *3*, e01641.
45. Rebelo, S.; Santos, M.; Martins, F.; e Silva, E. F. d. C.; e Silva, O. A. d. C., Protein phosphatase 1 is a key player in nuclear events. *Cellular signalling* **2015,** *27* (12), 2589-2598.
46. MacCallum, D. E.; Hall, P. A., Biochemical characterization of pKi67 with the identification of a mitotic-specific form associated with hyperphosphorylation and altered DNA binding. *Experimental cell research* **1999,** *252* (1), 186-198.

47. Cuylen, S.; Blaukopf, C.; Politi, A. Z.; Müller-Reichert, T.; Neumann, B.; Poser, I.; Ellenberg, J.; Hyman, A. A.; Gerlich, D. W., Ki-67 acts as a biological surfactant to disperse mitotic chromosomes. *Nature* **2016,** *535* (7611), 308-312.
48. Takagi, M.; Natsume, T.; Kanemaki, M. T.; Imamoto, N., Perichromosomal protein Ki67 supports mitotic chromosome architecture. *Genes to Cells* **2016,** *21* (10), 1113-1124.
49. Sobecki, M.; Mrouj, K.; Camasses, A.; Parisis, N.; Nicolas, E.; Lleres, D.; Gerbe, F.; Prieto, S.; Krasinska, L.; David, A., The cell proliferation antigen Ki-67 organises heterochromatin. *elife* **2016,** *5*, e13722.
50. Saiwaki, T.; Kotera, I.; Sasaki, M.; Takagi, M.; Yoneda, Y., In vivo dynamics and kinetics of pKi-67: transition from a mobile to an immobile form at the onset of anaphase. *Experimental Cell Research* **2005,** *308* (1), 123-134.
51. MacCallum, D. E.; Hall, P. A., The biochemical characterization of the DNA binding activity of pKi67. *The Journal of Pathology* **2000,** *191* (3), 286-298.
52. Bridger, J. M.; Kill, I. R.; Lichter, P., Association of pKi-67 with satellite DNA of the human genome in early G1 cells. *Chromosome Research* **1998,** *6* (1), 13-24.
53. Kill, I. R., Localisation of the Ki-67 antigen within the nucleolus: evidence for a fibrillarin-deficient region of the dense fibrillar component. *Journal of cell science* **1996,** *109* (6), 1253-1263.
54. Manoir, S. D.; Guillaud, P.; Camus, E.; Seigneurin, D.; Brugal, G., Ki-67 labeling in postmitotic cells defines different Ki-67 pathways within the 2c compartment. *Cytometry: The Journal of the International Society for Analytical Cytology* **1991,** *12* (5), 455-463.
55. Starborg, M.; Gell, K.; Brundell, E.; Höög, C., The murine Ki-67 cell proliferation antigen accumulates in the nucleolar and heterochromatic regions of interphase cells and at the periphery of the mitotic chromosomes in a process essential for cell cycle progression. *Journal of cell science* **1996,** *109* (1), 143-153.
56. Verheijen, R.; Kuijpers, H.; Driel, R. v.; Beck, J.; Dierendonck, J. v.; Brakenhoff, G.; Ramaekers, F., Ki-67 detects a nuclear matrix-associated proliferation-related antigen: II. Localization in mitotic cells and association with chromosomes. *Journal of Cell Science* **1989,** *92* (4), 531-540.
57. Ishida, S.; Huang, E.; Zuzan, H.; Spang, R.; Leone, G.; West, M.; Nevins, J. R., Role for E2F in control of both DNA replication and mitotic functions as revealed from DNA microarray analysis. *Molecular and cellular biology* **2001,** *21* (14), 4684-4699.
58. Ren, B.; Cam, H.; Takahashi, Y.; Volkert, T.; Terragni, J.; Young, R. A.; Dynlacht, B. D., E2F integrates cell cycle progression with DNA repair, replication, and G2/M checkpoints. *Genes & development* **2002,** *16* (2), 245-256.
59. Ishihara, M.; Mukai, H.; Nagai, S.; Onozawa, M.; Nihei, K.; Shimada, T.; Wada, N., Retrospective analysis of risk factors for central nervous system metastases in operable breast cancer: effects of biologic subtype and Ki67 overexpression on survival. *Oncology* **2013,** *84* (3), 135-140.
60. Sun, X.; Kaufman, P. D., Ki-67: more than a proliferation marker. *Chromosoma* **2018,** *127* (2), 175-186.
61. Polley, M.-Y. C.; Leung, S. C.; McShane, L. M.; Gao, D.; Hugh, J. C.; Mastropasqua, M. G.; Viale, G.; Zabaglo, L. A.; Penault-Llorca, F.; Bartlett, J. M., An international Ki67 reproducibility study. *Journal of the National Cancer Institute* **2013,** *105* (24), 1897-1906.

62. Trams, E. G.; Lauter, C. J.; Salem, J. N.; Heine, U., Exfoliation of membrane ecto-enzymes in the form of micro-vesicles. *Biochimica et Biophysica Acta (BBA)-Biomembranes* **1981,** *645* (1), 63-70.
63. Couch, Y.; Buzàs, E. I.; Di Vizio, D.; Gho, Y. S.; Harrison, P.; Hill, A. F.; Lötvall, J.; Raposo, G.; Stahl, P. D.; Théry, C., A brief history of nearly EV-erything–The rise and rise of extracellular vesicles. *Journal of extracellular vesicles* **2021,** *10* (14), e12144.
64. Islek, Z.; Bozkurt, B. T.; Ucisik, M. H.; Sahin, F., The role of extracellular vesicles in immunomodulation and pathogenesis of Leishmania and other protozoan infections. In *Extracellular Vesicles-Role in diseases, pathogenesis and therapy*, IntechOpen: 2022.
65. Logozzi, M.; Mizzoni, D.; Di Raimo, R.; Fais, S., Exosomes: a source for new and old biomarkers in cancer. *Cancers* **2020,** *12* (9), 2566.
66. Akers, J. C.; Gonda, D.; Kim, R.; Carter, B. S.; Chen, C. C., Biogenesis of extracellular vesicles (EV): exosomes, microvesicles, retrovirus-like vesicles, and apoptotic bodies. *Journal of neuro-oncology* **2013,** *113* (1), 1-11.
67. Van Niel, G.; d'Angelo, G.; Raposo, G., Shedding light on the cell biology of extracellular vesicles. *Nature reviews Molecular cell biology* **2018,** *19* (4), 213-228.
68. Pan, B.-T.; Teng, K.; Wu, C.; Adam, M.; Johnstone, R. M., Electron microscopic evidence for externalization of the transferrin receptor in vesicular form in sheep reticulocytes. *The Journal of cell biology* **1985,** *101* (3), 942-948.
69. Zhang, K.; Yue, Y.; Wu, S.; Liu, W.; Shi, J.; Zhang, Z., Rapid capture and nondestructive release of extracellular vesicles using aptamer-based magnetic isolation. *ACS sensors* **2019,** *4* (5), 1245-1251.
70. Pedersen, K. W.; Kierulf, B.; Neurauter, A., Specific and generic isolation of extracellular vesicles with magnetic beads. In *Extracellular Vesicles: Methods and Protocols*, Springer: 2017; pp 65-87.
71. Cheng, J.; Wang, X.; Yuan, X.; Liu, G.; Chu, Q., Emerging roles of exosome-derived biomarkers in cancer theranostics: messages from novel protein targets. *American Journal of Cancer Research* **2022,** *12* (5), 2226.
72. Kowal, J.; Arras, G.; Colombo, M.; Jouve, M.; Morath, J. P.; Primdal-Bengtson, B.; Dingli, F.; Loew, D.; Tkach, M.; Théry, C., Proteomic comparison defines novel markers to characterize heterogeneous populations of extracellular vesicle subtypes. *Proceedings of the National Academy of Sciences* **2016,** *113* (8), E968-E977.
73. Sina, A. A. I.; Vaidyanathan, R.; Wuethrich, A.; Carrascosa, L. G.; Trau, M., Label-free detection of exosomes using a surface plasmon resonance biosensor. *Analytical and bioanalytical chemistry* **2019,** *411* (7), 1311-1318.
74. Li, G.; De Clercq, E., Therapeutic options for the 2019 novel coronavirus (2019-nCoV). *Nature reviews Drug discovery* **2020,** *19* (3), 149-150.
75. Yang, H.; Rao, Z., Structural biology of SARS-CoV-2 and implications for therapeutic development. *Nature Reviews Microbiology* **2021,** *19* (11), 685-700.
76. Chilamakuri, R.; Agarwal, S., COVID-19: Characteristics and therapeutics. Cells. 2021; 10: 206. s Note: MDPI stays neutral with regard to jurisdictional claims in published …: 2021.
77. Walls, A. C.; Park, Y.-J.; Tortorici, M. A.; Wall, A.; McGuire, A. T.; Veesler, D., Structure, function, and antigenicity of the SARS-CoV-2 spike glycoprotein. *Cell* **2020,** *181* (2), 281-292. e6.

78. Carter, L. J.; Garner, L. V.; Smoot, J. W.; Li, Y.; Zhou, Q.; Saveson, C. J.; Sasso, J. M.; Gregg, A. C.; Soares, D. J.; Beskid, T. R., Assay techniques and test development for COVID-19 diagnosis. ACS Publications: 2020.
79. Gao, S.; Cheng, Y.; Zhang, S.; Zheng, X.; Wu, J., A biolayer interferometry-based, aptamer–antibody receptor pair biosensor for real-time, sensitive, and specific detection of the disease biomarker TNF-α. *Chemical Engineering Journal* **2022,** *433*, 133268.
80. Filius, M.; Fasching, L.; van Wee, R.; Rwei, A. Y.; Joo, C., Decoding aptamer-protein binding kinetics for continuous biosensing using single-molecule techniques. *Science Advances* **2025,** *11* (7), eads9687.
81. Bates, T. A.; Gurmessa, S. K.; Weinstein, J. B.; Trank-Greene, M.; Wrynla, X. H.; Anastas, A.; Anley, T. W.; Hinchliff, A.; Shinde, U.; Burke, J. E., Biolayer interferometry for measuring the kinetics of protein–protein interactions and nanobody binding. *Nature protocols* **2025,** *20* (4), 861-883.
82. Gerdes, J.; Lemke, H.; Baisch, H.; Wacker, H.-H.; Schwab, U.; Stein, H., Cell cycle analysis of a cell proliferation-associated human nuclear antigen defined by the monoclonal antibody Ki-67. *The journal of immunology* **1984,** *133* (4), 1710-1715.
83. Endl, E.; Gerdes, J., The Ki-67 protein: fascinating forms and an unknown function. *Experimental cell research* **2000,** *257* (2), 231-237.
84. Cattoretti, G.; Becker, M. H.; Key, G.; Duchrow, M.; Schlüuter, C.; Galle, J.; Gerdes, J., Monoclonal antibodies against recombinant parts of the Ki-67 antigen (MIB 1 and MIB 3) detect proliferating cells in microwave-processed formalin-fixed paraffin sections. *The Journal of pathology* **1992,** *168* (4), 357-363.
85. Hao, L.; Liu, L.; Meng, X.; Cui, H.; Wang, Z., Electrochemical analysis of Ki67 protein as pancreatic cancer biomarker based on graphene-polydopamine nanocomposite. *International Journal of Electrochemical Science* **2017,** *12* (4), 3040-3049.
86. Sun, Y.; Yang, K.; Bridal, T.; Ehrhardt, A. G., Robust Ki67 detection in human blood by flow cytometry for clinical studies. *Bioanalysis* **2016,** *8* (23), 2399-2413.
87. Kim, S.; Kim, S.; Ko, C.; Lee, W.; Kim, H. D., A microfluidic electrochemical immunosensor for detection of CEA and Ki67 in 3D tumor spheroids. *Materials Today Bio* **2025,** *32*, 101768.
88. Zhou, Q.; Rahimian, A.; Son, K.; Shin, D.-S.; Patel, T.; Revzin, A., Development of an aptasensor for electrochemical detection of exosomes. *Methods* **2016,** *97*, 88-93.
89. Ferreira, C.; Matthews, C.; Missailidis, S., DNA aptamers that bind to MUC1 tumour marker: design and characterization of MUC1-binding single-stranded DNA aptamers. *Tumor biology* **2006,** *27* (6), 289-301.
90. Alizadeh, F.; Yaghoobi, E.; Imanimoghadam, M.; Ramezani, M.; Alibolandi, M.; Abnous, K.; Taghdisi, S. M., Targeted delivery of epirubicin to cancerous cell using copper sulphide nanoparticle coated with polyarginine and 5TR1 aptamer. *Journal of Drug Targeting* **2023,** *31* (9), 986-997.
91. Théry, C.; Witwer, K. W.; Aikawa, E.; Alcaraz, M. J.; Anderson, J. D.; Andriantsitohaina, R.; Antoniou, A.; Arab, T.; Archer, F.; Atkin-Smith, G. K., Minimal information for studies of extracellular vesicles 2018 (MISEV2018): a position statement of the International Society for Extracellular Vesicles and update of the MISEV2014 guidelines. *Journal of extracellular vesicles* **2018,** *7* (1), 1535750.

92. Welsh, J. A.; Goberdhan, D. C.; O'Driscoll, L.; Théry, C.; Witwer, K. W., MISEV2023: An updated guide to EV research and applications. *Journal of extracellular vesicles* **2024,** *13* (2), e12416.
93. Song, Z.; Mao, J.; Barrero, R. A.; Wang, P.; Zhang, F.; Wang, T., Development of a CD63 aptamer for efficient cancer immunochemistry and immunoaffinity-based exosome isolation. *Molecules* **2020,** *25* (23), 5585.
94. Li, B.; Pan, W.; Liu, C.; Guo, J.; Shen, J.; Feng, J.; Luo, T.; Situ, B.; Zhang, Y.; An, T., Homogenous magneto-fluorescent nanosensor for tumor-derived exosome isolation and analysis. *ACS sensors* **2020,** *5* (7), 2052-2060.
95. Zhang, Z.; Tang, C.; Zhao, L.; Xu, L.; Zhou, W.; Dong, Z.; Yang, Y.; Xie, Q.; Fang, X., Aptamer-based fluorescence polarization assay for separation-free exosome quantification. *Nanoscale* **2019,** *11* (20), 10106-10113.
96. Poolsup, S.; Zaripov, E.; Hüttmann, N.; Minic, Z.; Artyushenko, P. V.; Shchugoreva, I. A.; Tomilin, F. N.; Kichkailo, A. S.; Berezovski, M. V., Discovery of DNA aptamers targeting SARS-CoV-2 nucleocapsid protein and protein-binding epitopes for label-free COVID-19 diagnostics. *Molecular Therapy Nucleic Acids* **2023,** *31*, 731-743.
97. Ahmed, N.; Francis, M. E.; Ahmed, N.; Kelvin, A. A.; Pezacki, J. P., MicroRNA-185 Inhibits SARS-CoV-2 Infection through the Modulation of the Host's Lipid Microenvironment. *Viruses* **2023,** *15* (9), 1921.
98. Xu, R.; Shi, M.; Li, J.; Song, P.; Li, N., Construction of SARS-CoV-2 virus-like particles by mammalian expression system. *Frontiers in bioengineering and biotechnology* **2020,** *8*, 862.
99. Yao, H.; Song, Y.; Chen, Y.; Wu, N.; Xu, J.; Sun, C.; Zhang, J.; Weng, T.; Zhang, Z.; Wu, Z., Molecular architecture of the SARS-CoV-2 virus. *Cell* **2020,** *183* (3), 730-738. e13.
100. Schoeffler, A. J.; Helgason, E.; Popovych, N.; Dueber, E. C., Diagnosing and mitigating method-based avidity artifacts that confound polyubiquitin-binding assays. *Biophysical reports* **2021,** *1* (2).
101. Wu, H.-B.; Wang, C.-H.; Chung, Y.-D.; Shan, Y.-S.; Lin, Y.-J.; Tsai, H.-P.; Lee, G.-B., Highly-specific aptamer targeting SARS-CoV-2 S1 protein screened on an automatic integrated microfluidic system for COVID-19 diagnosis. *Analytica chimica acta* **2023,** *1274*, 341531.
102. Song, Y.; Song, J.; Wei, X.; Huang, M.; Sun, M.; Zhu, L.; Lin, B.; Shen, H.; Zhu, Z.; Yang, C., Discovery of aptamers targeting the receptor-binding domain of the SARS-CoV-2 spike glycoprotein. *Analytical chemistry* **2020,** *92* (14), 9895-9900.
103. Schmitz, A.; Weber, A.; Bayin, M.; Breuers, S.; Fieberg, V.; Famulok, M.; Mayer, G., A SARS-CoV-2 spike binding DNA aptamer that inhibits pseudovirus infection by an RBD-independent mechanism. *Angewandte Chemie International Edition* **2021,** *60* (18), 10279-10285.
104. Cennamo, N.; Pasquardini, L.; Arcadio, F.; Lunelli, L.; Vanzetti, L.; Carafa, V.; Altucci, L.; Zeni, L., SARS-CoV-2 spike protein detection through a plasmonic D-shaped plastic optical fiber aptasensor. *Talanta* **2021,** *233*, 122532.